Predicting future wolf density in Scandinavia under land-use and climate scenarios with an individual-based hybrid model

Sinchan Ghosh[1,*], Oskar Franklin[1], Barbara Zimmermann[2]

[1] Agriculture, Forestry and Ecosystem Services Group, Biodiversity and Natural Resources Program, International Institute for Applied Systems Analysis (IIASA), Laxenburg, Austria

[2] Faculty of Applied Ecology, Agricultural Sciences and Biotechnology, Inland Norway University of Applied Sciences, Campus Evenstad, Koppang, Norway

[*] Corresponding author: Sinchan Ghosh, gsinchanpostdoc@gmail.com

Abstract

Managing wolves in Scandinavia requires projections of the density and distribution of territories under future land-use and climatic change. We coupled machine-learning estimators of deer availability, habitat suitability and the spatial pattern of human-caused mortality with a deterministic pack-level model of recruitment, dispersal, territory formation and territory size on a 50 × 50 km grid, and simulated Scandinavian wolf (*Canis lupus*) territories from 1999 to 2060 under five Shared Socioeconomic Pathways (SSPs). We tested whether territorial wolf density increases (H1a), decreases (H1b) or remains unchanged (H1c), and whether its distribution becomes more homogeneous (H2a), more heterogeneous (H2b) or remains unchanged (H2c). Without parameters fitted to the coupled trajectory, the model reproduced the colonisation of 1999–2015 (territories, $R^2 = 0.90$) and, out of sample, the plateau of 2016–2024 (84 simulated against 76 observed territories in 2024). Territories peaked at about 90 around 2040 and declined to 81–84 by 2060 under all pathways, while mean territory size fell from 807 to 596–666 km² and the density-weighted centroid moved from 59.9 to 57.6–58.0 °N. Territorial density increased under every pathway (H1a; SSP5-8.5: +16% in the last epoch relative to 1999–2015, Holm-adjusted $p < 0.001$). Its spatial heterogeneity was 16–19% higher than in the baseline but showed no significant trend under SSP5-8.5 (H2c) and increased significantly only under SSP1-1.9 and SSP1-2.6 (H2b). Regime-shift analysis identified three to four shifts, the last between 2027 and 2035, followed by a regime that persisted to 2060. Territory counts differed by 3% among pathways and density by 12%, and both the density increase and the southward shift depended on the spatial pattern of human-caused mortality. Wolf dynamics to 2060 are therefore governed by human-caused mortality and inbreeding rather than by climate.

Keywords: *Canis lupus*; agent-based model; territory dynamics; Crowley–Martin functional response; human-caused mortality; inbreeding; SSP scenarios; regime shifts; Scandinavia

1. Introduction

Grey wolves (*Canis lupus*) were nearly extinct in Scandinavia by the mid-1960s (Wabakken et al., 2001). After protection, wolves have recolonised it through dispersal and reproduction (Wabakken et al., 2001; Wikenros et al., 2021). By winter 2025-2026, there are up to 425 wolves, including 41 family groups and 30 pairs, with territories averaging 1,017 km² in size (Mattisson et al., 2013; Wabakken et al., 2026). Wolf predation on ungulates is perceived by hunters and farmers as a threat to the harvest of game and livestock (Wikenros et al., 2020; Zimmermann et al., 2014). This perceived threat motivates wolf culling and restricts the protected breeding range to the south of the reindeer husbandry areas (Milleret et al., 2017; Recio et al., 2018). In the breeding range, traffic collisions and illegal killing of wolves challenge wolf recolonisation and reduce the success of wolf protection (Recio et al., 2018; Milleret et al., 2022; Wabakken et al., 2026). Resolving wolf-human conflict involves managing a stable regime of wolf packs and territories in terms of density and distribution. Present management relies on monitoring that informs immediate and historical dynamics of packs and territories. A comprehensive stability and regime shift analysis of the wolf regime can inform the potential long-term success of the management policies under climatic scenarios. Such stability and regime shift analyses will require predicting the dynamics of density and distribution of Scandinavian wolf territories and packs in response to changes in their drivers.

Reproduction, survival and dispersal maintain a pack size of 4.3 ± 2.3 wolves in present-day Scandinavia (Mech & Boitani, 2003; Zimmermann et al., 2015). Each of these demographic processes varies in Scandinavian wolves with intrinsic and extrinsic factors. In each pack, a single breeding pair produces one litter, averaging 4.9 pups and reaching a maximum of nine pups per year (Axnér et al., 2023; Mech & Boitani, 2003; Nordli et al., 2023). Litter size declines by 1.15 pups for each 0.1 increase in the inbreeding coefficient in Scandinavian wolves (Liberg et al., 2005). About 70% of pups survive their first winter and become subadults (Liberg, Aronson, et al., 2012; Milleret et al., 2022). Overwinter pup survival is determined by the ratio of prey biomass acquired by the pack to the pack's total energy requirement (Zimmermann et al., 2015). Larger packs and lower prey accumulation reduce pup survival (Eberhardt, 2002; Zimmermann et al., 2015). Wolves follow a Crowley-Martin type predation, in which encounter rate, handling time and predation interference determine the prey biomass acquired (Zimmermann et al., 2015). Encounter rate rises with prey density and wolf movement inside the territory, which depends on the presence of clear cuts and gravel roads inside the territory. Handling time scales with prey size and vulnerability; e.g., wolves process roe deer and moose calves far faster than adult moose (Sand et al., 2012). Interference rises with pack size and with the presence of other predators such as brown bears in spring and exploitation competition in summer (Tallian et al., 2017, 2022).

Anthropogenic mortality is another driver of variability in overall pack survival. Most subadults then leave the natal territory at one to two years of age, and dispersal propensity declines in older cohorts (Mech & Boitani, 2003; Sanz-Pérez et al., 2018). In April, May and June, the whelping

of the next litter drives the primary dispersal, while competition with near-adult pups drives a second dispersal in autumn (Kojola et al., 2006; Sanz-Pérez et al., 2018). The dispersal distance varies from under 40 km to more than 200 km depending on the age of the disperser, density of territories, and availability of suitable habitat similar to the natal one (Kojola et al., 2006; Sanz-Pérez et al., 2018). Dispersed wolves pair up at mean ages of 2.0 and 2.4 years to form a new pack and establish a new territory, and the pairing lasts for around three consecutive winters (Milleret et al., 2017). Half of 153 monitored pairs dissolved within three winters, with two-thirds of them leaving no wolf on the territory (Milleret et al., 2017). Dissolution is caused primarily by the death of one or both breeders from legal culling, illegal poaching, and traffic collisions (Milleret et al., 2017).

Due to the risk of anthropogenic mortality, suitable habitat to host wolf territory is defined by the absence of human settlement and main roads (Ordiz et al., 2015; Recio et al., 2018). Forest cover, particularly coniferous forest, is one of the strongest determinants of habitat suitability (Recio et al., 2018; Zimmermann et al., 2014). However, gravel roads increase habitat permeability for patrolling larger territories without introducing mortality risk (Zimmermann et al., 2014). The territory size of wolves, like most territorial mammals, increases to compensate for resource scarcity, especially lower roe deer density in a habitat (Mitchell & Powell, 2004; Sells & Mitchell, 2020; Mattisson et al., 2013). Roe deer density and distribution vary with agriculture, snow depth, and forest cover. In opposition, resources with ubiquitous distribution, such as moose density, are limited in their predictive power for variability in habitat suitability (Mattisson et al., 2013). Management policy on wolf depredation risk on livestock adds a further boundary of habitat suitability to keep wolf breeding range outside the reindeer husbandry area (Eriksson & Dalerum, 2018; Recio et al., 2018; Trouwborst et al., 2017). While there is no reported direct impact of climate on wolf habitat suitability, the variability of land cover change across future climatic scenarios and the effect of snow depth on deer density and distribution suggest an indirect impact of climate on wolf habitat suitability.

Changing prey availability can alter reproduction (Eberhardt, 2002; Zimmermann et al., 2015), and changing habitat suitability can reshape dispersal patterns (Recio et al., 2018; Sanz-Pérez et al., 2018). Thus, the future regime of the distribution and density of wolf packs and territories may differ from the present one even under the same policies (Milleret et al., 2017; Recio et al., 2018). Increasing road density in developing urban areas across climatic scenarios can increase mortality in territorial and dispersing wolves (Recio et al., 2018; Zimmermann et al., 2014), but a higher availability of deer in warmer forests (Gervasi et al., 2013; Mattisson et al., 2013) and a decline in the inbreeding coefficient (Liberg et al., 2005; Åkesson et al., 2016) can compensate for the mortality through increased litter size and survival of pups (Eberhardt, 2002; Zimmermann et al., 2015). The variability in spatially explicit deer density, litter size, survival, and mortality can lead to (H1a) increased territorial wolf density, (H1b) decreased territorial wolf density, or (H1c) indifference across climatic scenarios relative to its current density. The changing land use and land cover can also lead to a different set of distributions of wolves' habitat suitability across climatic scenarios (Grilo et al., 2019; Recio et al., 2018). A greater expansion of agricultural landscape, reduced snow depth, or increased coverage of warmer forest can increase the roe deer density (Gervasi et al., 2013; Mattisson et al., 2013) enough to make it ubiquitous, losing

the heterogeneity in wolf habitat suitability distribution (Mattisson et al., 2013). In contrast, the changing forest cover and warming climate in southern Scandinavia can push the moose population towards northern Scandinavia (Bergqvist et al., 2018; Singh & Ericsson, 2014), introducing a new heterogeneity in habitat suitability for wolves. In such a case, across climatic scenarios, wolf territory and pack dynamics can result in (H2a) a more homogeneous distribution of wolves in the breeding range, (H2b) a more heterogeneous distribution of territorial wolves, or (H2c) an indifferent distribution pattern of wolf territories and packs across climatic scenarios. This study investigates "**how stable the regime of territorial wolves' density and distribution is under changing environments and current management**" by testing these hypotheses on Scandinavian wolves across climatic scenarios using known mechanisms of their demographic processes and predation discussed above.

2. Methodology

We built a hybrid model that couples mechanistic demographic and predation processes with machine-learning estimates of deer availability, habitat suitability and the spatial pattern of human-caused mortality. The model runs on a pack-level agent-based framework on a 50 × 50 km grid (EPSG:3035). The revised grid excludes Svalbard and the cells that lie entirely within the reindeer-husbandry area, leaving 213 mainland cells, of which the 212 with complete land-cover and snow inputs (cell centres 5.4–26.5 °E, 55.6–70.9 °N) form the model domain and the 204 with at least 10% land enter the statistical sub-models. This framework enables the simulation of differential dynamics among wolf packs in response to a spatially explicit, changing environment, so that the regime of territory density and distribution is an emergent property (Marucco & McIntire, 2010; Sells & Mitchell, 2020). Hybridising machine learning with the mechanistic model links climate-scenario-driven environmental data to the demographic and predation processes through habitat suitability, prey availability and mortality risk. These are conceptual indices of multiple environmental variables without established mechanisms for each variable, so machine-learning algorithms are a better choice to link the environment to demography and predation through latent, index-based variables (Elith et al., 2008; Elith & Leathwick, 2009). By contrast, each demographic and predation process is well studied, with established mechanisms for variability in its rates, so a mechanistic model is a better fit for the demographic and predation components (Milleret et al., 2017; Sanz-Pérez et al., 2018; Zimmermann et al., 2015). Section 2.1 describes the data, Section 2.2 the formulation of each part of the model, Section 2.3 the simulation experiments, Section 2.4 the regime-shift and stability analysis, and Section 2.5 the validation, assumption tests, sensitivity analyses and hypothesis tests.

2.1. Data

2.1.1. Monitoring records

We used annual winter monitoring data from the Norwegian and Swedish national programmes and the research project SKANDULV, covering 26 consecutive seasons from winter 1998/99 to 2023/24. The national programmes identify territorial wolves by combining snow tracking with

non-invasive genetic sampling (Åkesson et al., 2022). Each territory is delineated as a 100% minimum convex polygon around the genetic samples assigned to one pack, whereas SKANDULV delineates territories independently from the movements of GPS-collared wolves. Verified samples and territory records of the national programmes are downloaded from Rovbase, the joint Scandinavian carnivore database, and from the published annual status reports. Detection of territorial wolves and of reproduction is near-complete within the breeding range (Åkesson et al., 2022), whereas outside it the public and the authorities report sightings and tracks of single wolves to the open Skandobs portal. The data consist of four record types that differ in spatio-temporal extent and resolution. The Scandinavian annual summary gives, for each of the 26 seasons, the counts of territorial pairs and family groups, the total population estimates, the national breakdown with cross-border territories split equally, and the harvest and other mortality recorded in each country. The territory register gives 1,320 territory-winter records for 351 territories, comprising 784 family groups, 535 pairs and one single stationary wolf, each with a territory name, a report map number, a social status and a centre coordinate. The Norwegian and cross-border pack register gives 174 pack-years across 50 family-group territories, each with a minimum and maximum winter count, a confirmed reproduction flag, and the snow-tracking distance and observation days behind them. The SKANDULV telemetry register gives 93 pack-years across 39 territories for the wolf-years 1999 to 2020, each resting on at least nine months of tracking, of which we use the 100% minimum convex polygon (Mattisson et al., 2013). These data have coordinates in SWEREF 99 TM and in RT90 2.5 gon V, which we reprojected to EPSG:3035 and assigned to the cells of the revised grid by their centre. Per grid-year, we compiled the number of territories, the pack sizes, the territory sizes and the number of solitary wolves. Human-caused deaths (licensed hunting, protective culling, road and rail collisions, removals by the authorities and verified illegal killing) were retrieved with location, date and cause from Rovbase and assigned to cells and to the season between consecutive censuses; 890 such deaths fall within the revised grid in 1999–2024 (Section S6). Natural mortality and recruitment are not resolved at the territory scale in these records and are therefore modelled (Eqs. 3–4). We trained and parameterised the model on 1999–2015 and reserved 2016–2024 for validation. Telemetry ends in 2020, so territory size is available for only nine territories in the validation period, and 93% of the register territory sizes are imputed from latitude.

2.1.2. Environmental and deer data

Snow depth is the primary climatic predictor in our model, aggregated from daily values to the October–April mean and area-weighted to our 50 × 50 km grid. Historical values for 1999–2015 come from ERA5-Land (Muñoz-Sabater et al., 2021), and projections for 2016–2060 from EC-Earth3-Veg-LR under the five SSP–RCP scenarios of CMIP6 (Döscher et al., 2022). We expressed each projection as a change factor relative to its 1999–2015 baseline and applied it to the ERA5-Land climatology; over the overlap period 2016–2025, the harmonised projections agreed with ERA5-Land within 4–5% (mainland ratio 0.96–1.05, Spearman $\rho \geq 0.98$). We use land use and land cover (LULC) data from LUCAS LUC v1.1 (Hoffmann et al., 2023), which provide the annual fractional cover of the 16 LANDMATE plant functional types (Reinhart et al., 2022) at 0.1° resolution from 1950 to 2100 under CMIP6 SSP–RCP scenario combinations. We aggregated each 0.1° pixel

to the grid cells by area and calibrated urban and swamp cover against national land statistics (Section S2). We use the summed fraction of temperate deciduous trees, evergreen coniferous trees and deciduous coniferous trees (LANDMATE classes 4–6) to represent forest cover, the primary predictor of wolf territory occurrence and landscape refuge in Scandinavia (Recio et al., 2018) and a key habitat predictor of moose density (Gervasi et al., 2013). We use urban built-up land (class 15) to represent human settlement and main-road infrastructure, which lower wolf habitat suitability and inhibit pair establishment (Ordiz et al., 2015; Recio et al., 2018; Zimmermann et al., 2014). We use cropland (class 13) to represent agricultural land use, which lowers wolf habitat suitability (Recio et al., 2018) and, together with forest, forms the agricultural–forest mosaic that supports high roe deer density (Gervasi et al., 2013). Irrigated cropland (class 14) is negligible in Scandinavia and is merged with class 13 where both enter (Eq. 4.1.1); grassland used for hay and grazing falls in C3 grass (class 9). We use grid-level harvest rates of roe deer and moose calves to represent prey availability (Zimmermann et al., 2015). Roe deer density is the main predictor of wolf home-range size in Scandinavia (Mattisson et al., 2013). We obtained these harvest data from Viltdata for Sweden and from Statistics Norway and Hjorteviltregisteret for Norway, corrected them for reporting rates and land area, and harmonised municipal reforms (Section S2).

2.2. Model

2.2.1. Conceptual framework

Our agent-based modelling framework comprises four interconnected modules that track habitat suitability and prey availability, pack dynamics, distribution via dispersal, and the density of territories (Figure 1). This modular structure enables tracking uncertainty separately for each environmental and demographic process. A similar individual-based framework for wolf recolonisation was developed for the Western Italian Alps (Marucco & McIntire, 2010). However, that model assumes fixed habitat suitability, requires individual-level monitoring data for every wolf, and operates on a 1.56 km² raster with up to 100 movement steps per year. To overcome these monitoring and computational requirements, our framework operates at the pack level and considers spatio-temporal variability in habitat suitability, prey availability, mortality risk and demographic rates, and it derives the size of each territory from the space left by its neighbours.

Our model, especially the Habitat Module, rests on five assumptions based on the literature. In Scandinavia, snow depth shifts predation toward vulnerable calves (Sand et al., 2006a) and impairs the mobility of ungulates such as moose and roe deer, increasing their vulnerability to wolves (Kittle et al., 2017; Sand et al., 2006a). Therefore, the module assumes (A1) that snow depth provides greater habitat suitability to wolves by increasing the encounter rate of deer through their vulnerability, besides their density. The literature considers a range of human artefacts, from gravel roads and main roads to buildings, all of which except gravel roads have a negative impact on wolf settlement (Recio et al., 2018; Zimmermann et al., 2014). Since long-term projections for separate road classes are unavailable under future scenarios, the module assumes (A2) that the impact of these artefacts is captured by habitat suitability through the corresponding land-cover types. Harvest statistics provide a proxy for ungulate density but are

subject to bias in local harvest effort, efficacy and reporting. The module therefore uses a relative index of deer availability for spatial bias correction, assuming (A3) that the spatial distribution of these biases remains the same over time and across scenarios, given unchanged management policy. Sympatric brown bears reduce initial wolf pair establishment (Ordiz et al., 2015) and depress predation through interference (Zimmermann et al., 2015), but spatially explicit brown bear densities are unavailable for our study extent, and existing studies report the impact of brown bears in northern and central Scandinavia (Recio et al., 2018). The module therefore assumes (A4) that the competitive impact of brown bears is captured by the landscape covariates of northern and central Scandinavia. Finally, semi-domesticated reindeer husbandry in the north is subject to strict management policies and lethal removal of wolves to protect livestock, preventing pack establishment and territory persistence (Liberg, Aronson, et al., 2012; Recio et al., 2018). Our model assumes (A5) that cells lying entirely within the reindeer-husbandry area are unavailable to wolves and excludes them from the grid. In partly covered cells, only the land outside the husbandry area is available for territories, $GA_{eff}(g)$, and the human-caused mortality predicted for these cells is inflated by the removal policy (Eq. 4.1.3).

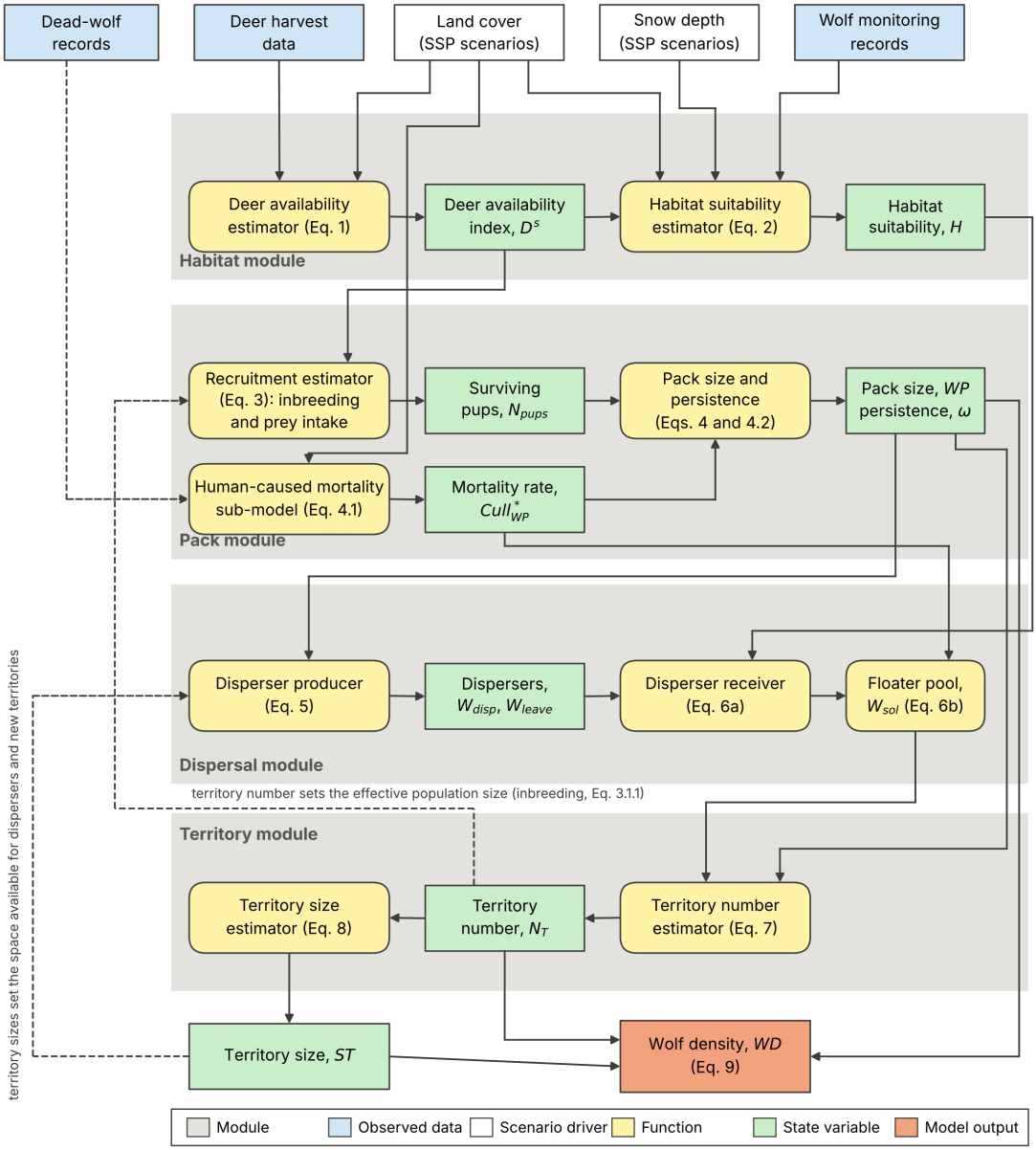


Figure 1. Schematic of the model. Observed data (blue) and scenario drivers (white) feed the functions (yellow) of the Habitat, Pack, Dispersal and Territory modules (grey), which update the state variables (green) and the model output, territorial wolf density (orange). Dashed lines show feedbacks from the observed or simulated territory state to the effective population size and to the space available for dispersers and new territories.

Habitat Module. The Habitat Module comprises the deer-availability estimator (Eq. 1) and the habitat-suitability estimator (Eq. 2). Equation 1 calculates the historical relative availability index of the two main prey from harvest data and projects it under the climatic scenarios from land-cover covariates. The effort was corrected by taking the ratio of harvest per area to the number of harvests reported, and the spatial relativity of harvest was calculated to account for the availability of each deer irrespective of its harvesting rate. We used roe deer and moose calves only, because moose calves are the main prey segment in Scandinavia, roe deer are the

main determinant of territory size, and moose alone constitute over 95% of wolf food biomass in summer, with roe deer the main alternative prey (Sand et al., 2016; Zimmermann et al., 2014). Eq. 1a transforms the species-specific, bias-corrected harvest rate, relative to its same-year mean over the mainland cells, into a relative deer-availability index bounded between 0 and 1 by min–max normalisation:

$$D_s(g,t) = \frac{Harv_s(g,t) - \min_{(g,t)\in T} Harv_s(g,t)}{\max_{(g,t)\in T} Harv_s(g,t) - \min_{(g,t)\in T} Harv_s(g,t)} \qquad \text{(Eq. 1a)}$$

where D_s(g,t) is the index of species s ∈ {roe deer, moose calves} in grid g and year t, $Harv_s$(g,t) is the relative harvest rate (animals per 1,000 ha per year relative to the same-year mean), and T is the set of grid-years of 1999–2015. The extrema are computed once over T, so the index can exceed 1 after 2015. Equations 1b and 1c are two competing estimators of D_s(g,t) from the fractional covers V_τ(g,t) of seven LANDMATE classes (4, 5, 7, 8, 9, 11 and 13; Gervasi et al., 2013), with no class removed by the variance-inflation criterion (VIF ≤ 10; Dormann et al., 2013). Eq. 1b is a beta regression (Ferrari & Cribari-Neto, 2004), fitted after the boundary adjustment $D'_s = [D_s(n-1) + 0.5]/n$ of Smithson and Verkuilen (2006):

$$D'_s(g,t) \sim \text{Beta}\left(\mu_s(g,t)\,\phi_s,\ [1-\mu_s(g,t)]\,\phi_s\right),$$
$$\text{logit}\,\mu_s(g,t) = \beta_{0s} + \sum_{\tau=1}^{7} \beta_{\tau s} V_\tau(g,t) \qquad \text{(Eq. 1b)}$$

and Eq. 1c is a random forest of B trees f_b with split parameters Θ_b:

$$\hat{D}_s(g,t) = \text{clip}_{[0,1]}\left\{\frac{1}{B}\sum_{b=1}^{B} f_b(\mathbf{V}(g,t);\Theta_b)\right\} \qquad \text{(Eq. 1c)}$$

Both were fitted by blocked cross-validation (whole year blocks crossed with 100 km spatial blocks), with the hyperparameters of the random forest selected by Bayesian optimisation (Section S3). The random forest was retained as the deer estimator because it had the lower cross-validated and validation error (Section 3.1); the beta regression was kept as the parametric comparator.

Equation 2 estimates habitat suitability H(g,t) ∈ [0,1], the relative probability that grid g holds wolf territories in year t. Presences are the grid-years of 1999–2015 with at least one territory (408 grid-years), and pseudo-absences are unoccupied grid-years of the same year drawn 1:1 (Barbet-Massin et al., 2012); a binary response gave higher cross-validated discrimination than continuous relative wolf density (AUC 0.81 against 0.74). H is the mean of gradient-boosting ensembles fitted to ten pseudo-absence draws,

$$H(g,t) = \frac{1}{10}\sum_{r=1}^{10} \mathrm{clip}_{[0,1]}\Big\{ \sum_{m=1}^{M_r} \nu_r\, h_{rm}(\mathbf{z}(g,t))\Big\},$$
$$\mathbf{z}(g,t) = \big(C(g,t),\, D_{roe}(g,t),\, L_{4\text{-}6},\, L_{12},\, L_{13},\, L_{15}\big) \qquad \text{(Eq. 2)}$$

where h_{rm} is the m-th regression tree of ensemble r, ν_r its learning rate, C(g,t) the snow depth, D_{roe}(g,t) the roe deer index of Eq. 1c, and L_k the fractional covers of forest (classes 4–6), swamp (12), cropland (13) and urban land (15). Snow depth enters in three parts separated by literature thresholds of 0.18 and 0.31 m, so that suitability can rise and then fall with snow, and monotone constraints impose a positive effect of forest, swamp and roe deer and a negative effect of cropland and urban land (Section S4). We fitted the ensembles with squared-error loss and selected their hyperparameters by Bayesian optimisation over the blocked cross-validation (Roberts et al., 2017; Valavi et al., 2019). Blocked cross-validation reduces but does not remove autocorrelation-driven inflation, so we treat predictive metrics as upper bounds on out-of-sample accuracy. To test algorithmic sensitivity, we fitted a generalised additive model to the same data and found no substantial difference in predictor importance or spatial pattern (Section S4).

Pack Module. This module takes the prey indices D_s(g,t) from the Habitat Module and calculates pack dynamics through density-dependent and predation-based mechanisms of reproduction, survival and dispersal. Reproduction and survival together define a recruitment function (Eq. 3), in which the reproductive output of each breeding pair is the proportion A(t) of its biotic potential retained under the inbreeding coefficient F(t), and the over-winter survival of pups is determined by the prey biomass the pack acquires. The number of pups recruited by pack j in grid g and year t is

$$N_{pups}(j,g,t) = Fecundity \times A(t) \times survival_{pups}(j,g,t) \qquad \text{(Eq. 3)}$$

where Fecundity = 9 pups pack^{-1} yr^{-1} is the maximum litter size recorded in Scandinavia (Axnér et al., 2023), and

$$A(t) = \max\big\{0,\ 1 - 1.76\,F(t)\big\} \qquad \text{(Eq. 3.1)}$$

is derived from the linear decline of litter size with the inbreeding coefficient reported by Liberg et al. (2005), with the max operator preventing negative litters (Section S5). The inbreeding coefficient is tracked with the Wright–Fisher approximation,

$$F(t) = F(t-1) + \frac{1 - F(t-1)}{2N_e(t)\,G}, \qquad N_e(t) = \frac{2\sum_g N_T(g,t)}{\kappa} \qquad \text{(Eqs. 3.1.1 and 3.1.1.1)}$$

where $2\Sigma_g N_T$(g,t) is the number of breeding wolves (two per territory), G = 4 years is the generation time, and κ = 2.5 is the variance-to-mean ratio of reproductive success (Frankham, 1995; Liberg et al., 2005). Although A(t) acts at pack level, N_e(t) is a population-level quantity across all packs in Scandinavia. The over-winter survival of pups depends on the prey biomass that the

pack acquires beyond the energetic needs of its older members,

$$survival_{pups}(j,g,t) = s_{nf}\ \min\left\{1,\ \max\left[0,\ \frac{Kill_W(j,g,t) - WP(j,g,t)\,B_{ad}\,T_W}{Fecundity\,B_{pup}}\right]\right\}$$

(Eq. 3.2)

where s_{nf} = 0.70 is the first-winter survival of pups when prey is not limiting (Liberg, Aronson, et al., 2012; Milleret et al., 2022), B_{ad} = 1.74 kg day^{-1} is the minimum daily intake of an adult, T_W = 212 days is the winter from October to April (Zimmermann et al., 2015), and B_{pup} = 667.8 kg is the minimum winter intake of a pup, derived from pup body mass and a starvation threshold of 0.09 kg kg^{-1} day^{-1} (Section S5). The denominator is the energetic demand of a maximum litter, so survival declines whenever the surplus kill cannot sustain it. The winter kill of pack j follows the Crowley–Martin functional response established for Scandinavian wolves (Zimmermann et al., 2015):

$$Kill_W(j,g,t) = B_{ad}\,T_W\,\frac{a\,D_B(g,t)\,P(j,g,t)}{[1 + a\,h\,D_B(g,t)][1 + c\,(P(j,g,t) - 1)]},$$
$$P(j,g,t) = WP(j,g,t) + Fecundity \qquad \text{(Eq. 3.2.1)}$$

Because roe deer and moose differ in edible biomass and each index is normalised to its own maximum, prey availability is expressed in adult rations per km²,

$$D_B(g,t) = \sum_s D_s(g,t)\,\frac{N_{s,max}\,B_s}{B_{ad}} \qquad \text{(Eq. 3.2.1.1)}$$

where $N_{s,max}$ is the density at D_s = 1 (7.8 roe deer km^{-2} and 2.36 moose km^{-2}, the latter scaling the mean of 1.3 moose km^{-2} inside wolf territories, Sand et al., 2016, to the median moose index of occupied cells) and B_s is the edible biomass per animal killed (15 kg for roe deer, 100 kg for moose). Zimmermann et al. (2015) fitted the Crowley–Martin model to winter kill rates of moose per wolf with faecal-pellet counts as the prey term; we converted their attack rate to moose density (a = 0.345 km² day^{-1}) and their handling time to rations (h = 0.0757 day ration^{-1}), and retained their interference coefficient (c = 0.42 wolf^{-1}). The rescaled function reproduces their observed range of winter kill rates and its decline with pack size (Section S5). Because pack sizes are integers (Eq. 4), the functional response is evaluated at the realised pack size.

Next, a pack-size calculator (Eq. 4) takes N_{pups}(j,g,t) as a discrete annual addition to the pack while deducting natural mortality, human-caused mortality and the dispersal of non-breeders. We chose a difference equation because the monitoring produces one observation per pack per winter census (Caswell, 2001), wolf reproduction is a seasonal pulse of one litter per pack in April–May (Caswell, 2001; Ledder et al., 2021), and all environmental inputs are annual (Jakeman et al., 2006). Pack size is tracked as

$$WP(j,g,t+1) = \text{round}\Big(\max\Big\{0,\, WP(j,g,t)\Big[1 - \frac{1}{Age_{death}} - Cull^{*}_{WP}(g,t)\Big] - [WP(j,g,t)-2]\frac{disprate}{Age_{dispersal}} + p_{breed}(\tau_j)\, N_{pups}(j,g,t)\Big\}\Big) \qquad \text{(Eq. 4)}$$

where $\text{Age}_{\text{death}}$ = 12 years is the life expectancy (Table S1), $\text{Age}_{\text{dispersal}}$ = 1.2 years is the mean age at dispersal, the mean of the Fennoscandian estimates (Chapron et al., 2016; Kojola et al., 2006; Sanz-Pérez et al., 2018), and disprate = 0.88 is the probability that a non-breeder disperses (Kojola et al., 2006), consistent with the near-complete dispersal by the age of two reported for Scandinavia (Chapron et al., 2016; Mattisson et al., 2013). The implied annual departure share of non-breeders, disprate/$\text{Age}_{\text{dispersal}}$ = 0.73, matches the share derived independently from the age structure of dispersers (0.755; Sanz-Pérez et al., 2018). N_{pups}(j,g,t) is weighted by the breeding probability $\text{p}_{\text{breed}}(\tau_{\text{j}})$, which is 0.79 in the first breeding season of a new pair (τ_{j} = 1) and 0.95 for established pairs ($\tau_{\text{j}} \geq 2$; Chapron et al., 2016). Because 1/$\text{Age}_{\text{death}}$ and Cull*_{WP}(g,t) are both shares of the wolves present at the census, the cause-specific rates are additive and act on the whole pack (Heisey & Fuller, 1985), whereas dispersal acts only on the non-breeding members, WP − 2. Pack sizes are integers, so the output of Eq. 4 is rounded, and a pack with fewer than two wolves is dissolved. None of these parameters was fitted.

The human-caused mortality rate Cull*_{WP}(g,t) is the share of the wolves present at census t that die of human causes before census t + 1. Over the training period, cells with monitored wolves take the observed Rovbase rate, Cull_{obs}(g,t), i.e. the human-caused deaths in the cell divided by the wolves present at the census (Section S6). All other grid-years, and all years after 2015, take the two-step sub-model

$$Cull^{*}_{WP}(g,t) = \text{clip}_{[0,1]}\Big\{\bar{c}(t)\,\frac{P(g,t)}{\bar{P}_{occ}(t)}\,f_{RH}(g) + c_{cr}\,\frac{P(g,t)}{\bar{P}_{occ}(t)}\Big\} \qquad \text{(Eq. 4.1)}$$

where the first term redistributes the national mean rate $\bar{\text{c}}$(t) in proportion to the relative probability P(g,t) of observing a human-caused death, and the second adds cryptic mortality (below). P(g,t) is the mean of ten LightGBM classifiers, each trained on the cell-years with at least one human-caused death in 1999–2015 and one same-year 1:1 draw of cell-years without deaths (Barbet-Massin et al., 2012), with the fractional covers L(g,t) of eleven LANDMATE classes as predictors,

$$P(g,t) = \frac{1}{10}\sum_{r=1}^{10} f_r(\mathbf{L}(g,t)) \qquad \text{(Eq. 4.1.1)}$$

and $\bar{\text{P}}_{\text{occ}}$(t) is the wolf-weighted mean of P over the occupied cells of year t, so that the redistribution preserves the national mean rate. A regression of the rate itself on land cover explained

0.2% of its deviance, because licensed hunts and protective culls remove whole packs and make deaths about three times more clustered than chance; the occurrence of deaths, by contrast, is predictable from land cover (Section S6; Recio et al., 2018). The national rate is the observed wolf-weighted mean until 2015 and thereafter follows the national population size,

$$\bar{c}(t) = \begin{cases} \dfrac{\sum_g D_{anth}(g,t)}{\sum_g W(g,t)}, & t \le 2015 \\ \bar{c}_0 + \bar{c}_1\, N(t), & t > 2015 \end{cases},$$

$$\bar{c}_0 = 0.0305, \;\; \bar{c}_1 = 0.000148 \text{ wolf}^{-1} \qquad \text{(Eq. 4.1.2)}$$

which captures the policy-driven increase in culling as the population grows. Calibrated on 1999–2014, Eq. 4.1.2 predicts the 2015–2023 mean rate (0.097 against 0.097 observed). Removals in and near the reindeer-husbandry area raise mortality in partly covered cells, which we represent by the saturating inflation

$$f_{RH}(g) = 1 + 1.76\Big[1 - \exp\Big(-\frac{rh_g}{0.03}\Big)\Big] \qquad \text{(Eq. 4.1.3)}$$

where rh_g is the husbandry share of the land of cell g; fitted to the 749 occupied cell-years of 1999–2023, the inflation reaches 95% of its maximum (× 2.76) at about 9% husbandry cover (Section S7). It applies only to predicted rates, because observed Rovbase rates already contain this effect.

Illegal killing is subject to imperfect and spatially non-uniform detection (Liberg, Chapron, et al., 2012). We estimated the cryptic mortality of pack wolves, c_{cr} = 0.04 yr^{-1} (range 0–0.06), from the population balance between successive censuses, recruitment (Eq. 3), recorded deaths and natural mortality, restricted to pack wolves so that the mortality of floaters, represented separately in Eq. 6b, is not counted twice (Section S8). Each territory carries an expected persistence

$$\omega_j(t+1) = \omega_j(t)\, \max\Big\{0,\; 1 - \frac{1}{Age_{death}} - Cull^{*}_{WP}(g,t)\Big\},$$

$$\omega_j(t_0) = 1; \quad \omega_j = 0 \text{ if } WP(j,g,t+1) < 2 \qquad \text{(Eq. 4.2)}$$

so that the expected number of territories in grid g is $N_T(g,t) = \Sigma_j\, \omega_j(t)$. A territory is thus lost at the per-capita rate of breeder mortality, which reproduces the observed annual dissolution rate (0.20–0.25) without an additional parameter (Section S8).

Dispersal Module. This module sums the dispersers produced by all packs, allocates those leaving their natal grid among the other grids, and maintains the floater (solitary wolf) pool from which new territories form. The disperser producer sums the dispersers of all packs in grid g,

$$W_{disp}(g,t) = \sum_j \omega_j(t)\,[WP(j,g,t) - 2]\,\frac{disprate}{Age_{dispersal}} \qquad \text{(Eq. 5.1)}$$

of which a share leaves the grid,

$$W_{leave}(g,t) = \left[1 - p_{stay}(g,t)\right] W_{disp}(g,t),$$
$$p_{stay}(g,t) = \begin{cases} 1, & ST_{required}(g,t) = 0 \\ \min\left\{1, \dfrac{ST_{available}(g,t)}{ST_{required}(g,t)}\right\}, & ST_{required}(g,t) > 0 \end{cases} \qquad \text{(Eqs. 5, 5.2 and 5.2.1)}$$

The space available for new territories is the land outside the reindeer-husbandry area not yet covered by territories, and the space required is the pair-equivalent demand of the dispersers at the minimum territory size,

$$ST_{available}(g,t) = \max\left\{0,\ GA_{eff}(g) - \sum_j \omega_j(t)\, ST(j,g,t)\right\},$$
$$ST_{required}(g,t) = S_{min}\,\frac{W_{disp}(g,t)}{2} \qquad \text{(Eqs. 5.2.1.1 and 5.2.1.2)}$$

where $GA_{eff}(g)$ is the land area of grid g outside the reindeer-husbandry area. The spacing between territories is represented by the buffer of Eq. 8.0, so no packing coefficient is applied here. Following natal-habitat-biased dispersal (Sanz-Pérez et al., 2018), the dispersers leaving grid h are allocated among the other grids g in proportion to their available space, the suitability of g and its similarity to the natal habitat, and the inverse of the distance between them:

$$W_{new}(g,t) = W_{disp}(g,t)\, p_{stay}(g,t) + \sum_{h \neq g} \omega(h \to g, t)\, W_{leave}(h,t),$$
$$\omega(h \to g, t) = \frac{ST_{available}(g,t)\, \Delta H(g,h,t)/d_{h\to g}}{\sum_{k \neq h} ST_{available}(k,t)\, \Delta H(k,h,t)/d_{h\to k}},$$
$$\Delta H(g,h,t) = H(g,t)\left[1 - |H(g,t) - H(h,t)|\right] \qquad \text{(Eq. 6a)}$$

Distances between grid centres, $d_{h\to g}$, are capped at 1,000 km, the maximum dispersal distance reported for Scandinavian wolves (Kojola et al., 2006; Wabakken et al., 2001); dispersers without a receiving grid within this distance are treated as emigrating or dying. Eq. 6b tracks the floater pool of each grid, to which newly arrived dispersers are added and from which surviving floaters leave by pairing:

$$W_{solitary}(g,t+1) = W_{new}(g,t) + W_{solitary}(g,t)\left[1 - \mu_F(g,t)\right] - 2\,\Delta N_{T,new}(g,t),$$
$$\mu_F(g,t) = \mu_0 + Cull^*_{WP}(g,t) \qquad \text{(Eq. 6b)}$$

The carry-over captures the one to two years between natal dispersal and territory establishment in Scandinavian wolves (Milleret et al., 2017). Floater mortality combines a background rate μ_0 = 0.376 yr^{-1} with the local human-caused rate, and μ_0 is set so that the floater-weighted national mean equals μ_F = 0.5 (Milleret et al., 2022; Section S11). At initialisation, the pool of each grid

is the number of solitary wolves recorded in winter 1998/99.

Territory Module. This module tracks the number N_T(g,t) and size ST(j,g,t) of territories per grid to calculate the territorial wolf density WD(g,t). A territory number calculator (Eq. 7) adds the new territories that survive their first year to the persisting ones:

$$N_T(g,t+1) = \sum_j \omega_j(t+1) + \Delta N_{T,new}(g,t)\Big[1 - \frac{1}{Age_{death}} - Cull^*_{WP}(g,t)\Big] \qquad \text{(Eq. 7)}$$

New territories form when floaters of opposite sex and breeding age meet, limited by the space available:

$$\begin{aligned} &\Delta N_{T,new}(g,t) = \min\big\{X(g,t),\ n_{cap}(g,t)\big\},\\ &X(g,t) \sim \text{Binomial}\,\big(n(g,t),\ P_B\big),\\ &E[n(g,t)] = \frac{W_{solitary}(g,t)}{2} \qquad \text{(Eq. 7.1)} \end{aligned}$$

$$\begin{aligned} &P_B = \min\Big\{1, \frac{1}{2.0-1.2}\Big\}\ \min\Big\{1, \frac{1}{2.4-1.2}\Big\} \times 0.5 = 0.42,\\ &n_{cap}(g,t) = \Big\lfloor \frac{ST_{available}(g,t)}{S_{min}} \Big\rfloor \qquad \text{(Eq. 7.2)} \end{aligned}$$

The number of potential pairs n(g,t) is half the floater pool, rounded stochastically so that its expectation is $W_{solitary}/2$. P_B is the annual probability that a potential pair forms a territory: for each sex, the reciprocal of the waiting time between the age at dispersal (1.2 years) and the mean age at pairing (2.0 years for males and 2.4 years for females; Milleret et al., 2017), capped at one, multiplied by the probability that the two floaters are of opposite sex (0.5). Eq. 7.1 is the only stochastic process of the model; the expected-value run replaces X(g,t) by P_B $W_{solitary}/2$.

The territory size estimator (Eq. 8) updates the size of existing territories and sets the size of new ones from the space their neighbours leave. Each territory occupies its area plus a buffer of width b around it,

$$\begin{aligned} &\eta_j = \frac{\pi\,(r_j + b)^2}{ST(j,g,t)},\\ &r_j = \sqrt{ST(j,g,t)/\pi},\\ &ST_{av}(g,t) = GA_{eff}(g) - \sum_j \omega_j\,\eta_j\,ST(j,g,t) \qquad \text{(Eq. 8.0)} \end{aligned}$$

and an existing territory moves towards the size it would claim without neighbours, $\bar{S}$, as far as the free space shared equally among the territories of the grid allows:

$$ST_{target}(j,g,t) = \text{clip}\,\Big(\ \min\Big\{\bar{S},\ ST(j,g,t) + \frac{ST_{av}(g,t)}{N_T(g,t)}\Big\},\ S_{min},\ S_{max}\Big) \qquad \text{(Eq. 8.1)}$$

$$ST(j,g,t+1) = ST(j,g,t) + \lambda\left[ST_{target}(j,g,t) - ST(j,g,t)\right] \qquad \text{(Eq. 8b)}$$

New territories share the free space of Eq. 5.2.1.1 equally:

$$ST_{new}(g,t) = \text{clip}\left(\min\left\{\bar{S},\ \frac{ST_{available}(g,t)}{\Delta N_{T,new}(g,t)}\right\},\ S_{min},\ S_{max}\right) \qquad \text{(Eq. 8a)}$$

Here, $\bar{S}$ = 1,017 km², S_{min} = 259 km² and S_{max} = 1,676 km² are the mean, minimum and maximum of 63 annual 100% minimum convex polygons of Scandinavian wolf territories (Mattisson et al., 2013). Free space thus allows expansion towards $\bar{S}$, and a negative ST_{av}, a grid overfilled by infilling, forces a compression shared among its territories. The buffer b = 2 km and the relaxation rate λ = 0.15 were fitted to 34 consecutive-year pairs of telemetry territories in 1999–2014 (Section S12); at λ = 0.15, a territory closes half of its gap to the target in about four years. We did not let territory size decrease with habitat suitability, because telemetry territories were larger, not smaller, where H was higher (ρ = +0.47, p = 0.001), and every H-based size rule predicted territory size worse than a constant (Section S12). Habitat suitability therefore governs where territories form (Eqs. 6a and 7), not how large they are. New territories use the unbuffered space of Eq. 5.2.1.1, which reproduced the territory sizes and densities of 1999–2024 better than the buffered space of Eq. 8.0 (Section 3.7).

Territorial wolf density per grid, the primary output, is the persistence-weighted ratio of pack wolves to territory area:

$$WD(g,t) = \frac{\sum_j \omega_j(t)\, WP(j,g,t)}{\sum_j \omega_j(t)\, ST(j,g,t)} \qquad \text{(Eq. 9)}$$

2.3. Simulation protocol

The model was simulated at an annual winter-to-winter step, with t indexing the winter census, from 1999 to 2060. The simulation was initialised with the observed state of winter 1998/99: the 10 territories of the register with their pack sizes and territory sizes (clipped to [S_{min}, S_{max}]), the solitary wolves of each grid, and F(0) = 0.184, the value at which Eq. 3.1.1, driven by the observed territory count, gives F(2015) = 0.25 (Laikre et al., 2016). Over 1999–2015, all runs share the historical forcing: habitat suitability (Eq. 2) and the mortality pattern (Eq. 4.1.1) from historical land cover and ERA5-Land snow, the observed deer-availability index (Eq. 1a), and the observed Rovbase mortality where wolves were monitored. From 2016, H(g,t) and P(g,t) follow the land cover and snow of each SSP, the deer index is the observed one where harvest data exist (to 2024) and the Eq. 1c projection thereafter, and human-caused mortality follows Eqs. 4.1–4.1.3. The years 2016–2024 are therefore an out-of-sample validation, reported as the mean of the five SSPs, and 2025–2060 the projection. Within each step, the Pack (Eqs. 3–4.2), Dispersal (Eqs. 5–6b) and Territory (Eqs. 7–8) modules were executed in sequence before WD(g,t) (Eq. 9) was computed. Because territory establishment (Eq. 7.1) is the only stochastic process, each SSP was run for R = 500 replicates with common random seeds, together with one expected-value run; the

standard error of the replicate-mean territory count was below 0.8% of the mean in every year and 0.3% in 2060, within the 1% criterion (Lee et al., 2015). Outputs are reported as replicate means with 95% percentile envelopes. All demographic, energetic and dispersal parameters were fixed at literature values (Table S1), and the statistical sub-models (Eqs. 1, 2 and 4.1) and the parameters without a direct literature value (c_{cr}, μ_0, b, λ, $\bar{c}_0$, $\bar{c}_1$ and the husbandry inflation) were each fitted independently against the data of the process they govern within 1999–2015 (Sections S3–S12; Grimm et al., 2005). No parameter was fitted to the coupled trajectory.

2.4. Regime shift and stability analysis

We define an ecological regime as a persistent, dynamic state around which the density and distribution of territorial wolves fluctuate until an abrupt shift takes them to a contrasting state (Scheffer & Carpenter, 2003). The annual, spatially explicit territorial wolf density, WD(g,t), must therefore be summarised as a vector state that captures where wolf territories are and how densely they are occupied, with persistence evaluated from the temporal dynamics of this vector. Such vectors for the spatial distribution and density of animal populations are described by largely independent axes of location, quantity, occupancy and aggregation (Rufino et al., 2018; Woillez et al., 2009). We therefore defined the regime state as the vector $z_t = (C_t, \bar{D}_t, O_t, CV_{WD,t})$. Here, C_t is the density-weighted latitudinal centroid of the territorial wolf distribution, an indicator of range shifts (Perry et al., 2005). $\bar{D}_t$ is the mean territorial wolf density across occupied grids, weighted by the probability that a grid is occupied, which describes how densely the occupied range is used (Bischof et al., 2020). O_t is the expected number of occupied grids ($N_T(g,t) \geq 1$), which describes the extent of the occupied range (Gaston et al., 2000). $CV_{WD,t}$ is the coefficient of variation of territorial wolf density among occupied grids, which describes the spatial heterogeneity of density independently of its mean (Taylor, 1961). Regime shifts were detected by applying the Sequential t-test Analysis of Regime Shifts (STARS; Rodionov, 2004), with a 5-year cut-off, to the first principal component of the standardised z_t, which summarises the vector's dominant multivariate trajectory (Möllmann et al., 2009). The stability of each detected regime was quantified from its duration and the behaviour of z_t within it. Persistence was defined as the duration of a regime in years (Pimm, 1984). Variability was defined as the mean Euclidean distance between the annual standardised z_t and the regime's mean state vector $\bar{z}_r$, with lower values indicating a more constant regime (Donohue et al., 2013). The magnitude of a regime shift was defined as the Euclidean distance between the mean state vectors of consecutive regimes, $\|\bar{z}_{r+1} - \bar{z}_r\|$. A regime was therefore considered more stable the longer it persisted and the less z_t varied within it. Shifts were detected on the replicate means of each SSP and on every replicate, and replicate metrics were summarised by the median and 90% interval. Because wolves in the model do not feed back on prey or vegetation, the detected regimes are forcing-driven persistent modes of wolf spatial organisation, not evidence of alternative stable states, hysteresis or trophic cascades.

2.5. Model evaluation and hypothesis testing

2.5.1. Model validation

Each statistical sub-model was evaluated by temporally and spatially blocked cross-validation on 1999–2015 (whole year blocks held out, spatial blocks of at least 100 km; Roberts et al., 2017) and against the withheld 2016–2024 data, and each process equation was tested against the data of the process it represents (Sections S3–S12). The coupled model was evaluated in two ways. In the free run, the model was simulated from the 1999 register, and its national series of territories, pack wolves, floaters, occupied grids, mean territory size and the regime-vector components (Section 2.4) were compared with the register for the training (2000–2015) and validation (2016–2024) periods by R^2, RMSE, bias and the ratio of observed to predicted totals; annual foundings and losses of territories were compared with the register flows, the grid-year occupancy probability by the area under the ROC curve (AUC), and the cell-mean territory count by Pearson's r. In the one-step test, each census year t was started from its observed state (territories, pack sizes, territory sizes, floaters, territory age and F(t) from the observed territory count) under the observed mortality, and the expected-value prediction for t + 1 was compared with the register.

2.5.2. Assumption tests

Module 1 rests on five assumptions (A1–A5; Section 2.2). A1, A2 and A4 were evaluated as comparisons between otherwise identical variants of Eq. 2 over the blocked cross-validation (10 pseudo-absence draws × 5 folds), with the out-of-sample RMSE as primary metric, R^2 and AUC as secondary metrics, and paired t-tests with Holm correction (Holm, 1979). For A1, the snow-depth variant was compared with a variant in which snow depth was replaced by latitude and elevation; A1 was supported if the snow-depth variant had at least 5% lower mean RMSE and no lower mean R^2. For A2, the full land-cover set was compared with a set without urban land and cropland, the classes representing settlements and main roads, under the same criterion. A3 was pre-specified as a test of the temporal stationarity of the spatial bias of the harvest index against independent deer censuses; this test could not be performed, because none of the 17 cells with censused territories (29 territory-years) was censused in both 1999–2007 and 2008–2015. A3 was therefore evaluated by a non-inferiority comparison of the Eq. 1 index with the observed index as predictor of Eq. 2, passed if the RMSE was not more than 5% higher and R^2 not more than 0.02 lower. For A4, forest (classes 4–6) and swamp (class 12), the land covers that represent northern and central Scandinavia, were removed from Eq. 2; A4 was flagged as sensitive if their removal changed projected habitat suitability by more than 10% in more than half of the forcing epochs. A5 was evaluated by sensitivity analysis (Section 2.5.3).

2.5.3. Sensitivity analysis

A one-at-a-time (OAT) analysis varied each of 19 parameters by ±20% ($Age_{dispersal}$, disprate, Age_{death}, Fecundity, the inbreeding-depression slope, s_{nf}, a, h, c, the scale of $Cull^*_{WP}$, $\bar{c}_1$, c_{cr}, μ_0, P_B, S_{min}, S_{max}, $\bar{S}$, b and λ) under SSP5-8.5 with R = 100 replicates and common seeds, and two-way factorial analyses (−20%, baseline, +20%) were run for $P_B \times \mu_0$, a × h and $\bar{S} \times \lambda$. The sensitivity of territory formation to the assumption that dispersers immediately contribute

to the local space demand was tested by setting the disperser-to-pair conversion factor of Eq. 5.2.1.2 to 0.3, representing delayed pairing of floaters, and 0.65. Initial-condition sensitivity was evaluated by perturbing the 1999 territory counts, pack sizes and territory sizes by ±20%, with a divergence of more than 10% from the baseline flagged. To evaluate A5, the model was re-run with the reindeer-husbandry area treated as suitable (whole land area available, no mortality inflation). Structural alternatives were the buffered space for new territories (Eq. 8.0 in Eq. 8a), Rovbase mortality to 2024 followed either by Eq. 4.1.2 or by the constant 1999–2024 mean rate, a constant national rate of 0.097 yr^{-1}, a spatially uniform mortality pattern ($P(g,t)/\bar{P}_{occ}$ = 1 after 2015), an inbreeding coefficient frozen from 2025, the Eq. 1c deer index from 2016, no husbandry inflation, and the refitted mortality pattern of the rebuilt Eq. 4.1. Global sensitivity was assessed by Latin-hypercube sampling (McKay et al., 1979) of 21 parameters within ±20% of their baseline values (200 samples × 10 replicates, SSP5-8.5), including scale factors on deer availability and habitat suitability, and by partial rank correlation coefficients (PRCC; Marino et al., 2008) between each parameter, grouped by module, and the 2060 states and the confirmatory trend slopes. Samples in which the population collapsed to fewer than two territories were excluded from the PRCC and reported separately. Runs in which the coefficient of variation of $\bar{D}_t$ across the final three forcing epochs exceeded 0.50 were to be flagged as numerically unstable.

2.5.4. Uncertainty analyses

Stochastic uncertainty is given by the 95% percentile envelopes of the replicates (Section 2.3). Because deer availability and habitat suitability enter the demographic modules as fixed inputs, their prediction uncertainty is not propagated through the model chain. Its effect on the confirmatory estimands was bounded by re-running the model with the lower and upper bounds of each input: the 2.5% and 97.5% percentiles of the tree predictions of the random forest (Eq. 1c) and of the ten members of the habitat-suitability ensemble (Eq. 2). A confirmatory test was flagged as inconclusive if the sign of its trend slope differed between the bounds, regardless of its p-value. This approximates, but does not replace, full hierarchical uncertainty propagation.

2.5.5. Confirmatory hypotheses

Each hypothesis of the Introduction was converted into one estimand, one test and one decision rule, specified before the projections were analysed (Table 1). H1 concerns the quantity axis of the regime vector, the mean territorial wolf density across occupied grids, $\bar{D}_t$, and H2 its heterogeneity axis, the coefficient of variation of territorial wolf density among occupied grids, $CV_{WD,t}$ (Section 2.4). Both were averaged over eight 6-year forcing epochs (2016–2021, …, 2052–2057 and the partial epoch 2058–2060), which are reporting units and do not define ecological regimes. Each hypothesis has three outcomes, so each was tested by a two-sided linear trend test of the epoch means of the replicate-mean series against the epoch midpoints, with the Holm–Bonferroni correction across H1 and H2 (Holm, 1979). SSP5-8.5 served as the confirmatory scenario, because it combines the strongest climate and land-use forcing, and the other four SSPs were reported as exploratory. The change relative to the 1999–2015 baseline, the share of replicates with a positive slope and a Mann–Kendall test were reported as supporting evidence. The regime-shift analysis (Section 2.4) and the trends of territory number, territory size, occupied

grids and centroid were exploratory.

Table 1. Pre-specified confirmatory hypotheses, estimands and decision rules.

	H1: territorial wolf density	**H2: distribution of territorial wolves**
Hypotheses	H1a: density increases; H1b: density decreases; H1c: no change	H2a: more homogeneous; H2b: more heterogeneous; H2c: no change
Estimand	Epoch mean of $\bar{D}_t$, the mean of WD(g,t) over occupied grids, weighted by the probability that the grid is occupied (wolves km^{-2})	Epoch mean of $CV_{WD,t}$, the coefficient of variation of WD(g,t) among occupied grids
Test	Two-sided linear trend test of the eight epoch means (slope β_D, 6 df)	Two-sided linear trend test of the eight epoch means (slope β_{CV}, 6 df)
Decision	H1a if Holm-adjusted $p < 0.05$ and the 95% CI of $\beta_D > 0$; H1b if $p < 0.05$ and CI < 0; otherwise H1c	H2b if Holm-adjusted $p < 0.05$ and the 95% CI of $\beta_{CV} > 0$; H2a if $p < 0.05$ and CI < 0; otherwise H2c
Multiplicity	Holm–Bonferroni across H1 and H2	Holm–Bonferroni across H1 and H2

Statistical power and minimum detectable effect. Each test uses n = 8 epoch means with midpoints treated as equally spaced (Δ = 6 years), leaving 6 residual degrees of freedom. Under the Holm correction, the most stringent two-sided level is $\alpha^* = 0.05/2 = 0.025$, with critical t = 2.97. With $\Sigma(x_i - \bar{x})^2 = n(n^2 - 1)\Delta^2/12 = 1{,}512$ yr^2, $SE(\beta) = \sigma_\varepsilon/38.9$, where σ_ε is the residual standard deviation of the estimand around the linear trend. At 80% power, the non-centrality parameter of the non-central t-distribution is 3.94, so the minimum detectable slope is $\beta_{min} = 0.101\ \sigma_\varepsilon$ yr^{-1}, a total change of 4.26 σ_ε over the 42 years between the first and last epoch midpoints. σ_ε was estimated from the three training epochs (1999–2004, 2005–2010, 2011–2015) of the replicate-mean series (Table 2).

Table 2. Minimum detectable effect (MDE) at 80% power.

Hypothesis	**Estimand**	**σ_ε (training epochs)**	**MDE: slope (yr^{-1})**	**MDE: change over 42 years**	**Relative to the 1999–2015 baseline**
H1	$\bar{D}$ (wolves km^{-2})	1.85×10^{-4}	1.88×10^{-5}	7.9×10^{-4}	15% of 5.11×10^{-3}; ecologically plausible, adequately powered
H2	CV_{WD}	0.044	4.5×10^{-3}	0.19	45% of 0.416; larger than plausible changes, underpowered

3. Results

3.1. Sub-model performance

Every sub-model was evaluated on its own data before coupling (Table 3). The random forest (Eq. 1c) predicted the deer-availability index better than the beta regression (Eq. 1b) for both species, and more so out of sample (validation R^2 0.77 against 0.40 for roe deer, 0.79 against 0.49 for moose calves), so it was retained as the deer estimator. Habitat suitability (Eq. 2) discriminated occupied from unoccupied grid-years with a blocked cross-validated AUC of 0.82 and

transferred to 2016–2024 under all five SSPs (AUC 0.85–0.86), with median H of 0.71 in occupied and 0.22 in unoccupied cells in 2016–2024. The occurrence of human-caused deaths (Eq. 4.1.1) was predicted with a temporal cross-validated AUC of 0.80 and a validation AUC of 0.84, but among occupied cells only with AUCs of 0.60 and 0.57, so P(g,t) separates where wolves can be killed from where they cannot better than it ranks the risk among occupied cells. The process equations reproduced the data of their processes without fitted parameters: the national pack size (Eq. 4) was unbiased in validation (−0.02 wolves), the dissolution rate (Eq. 4.2) was within 0.01 of the observed rate in training and 0.03 in validation, the inflow of new dispersers (Eq. 5) and the floater pool (Eq. 6b) were unbiased in validation (observed/predicted 0.99 and 1.02), and new territories (Eq. 7) were unbiased in the one-step test (1.04). The target size of Eq. 8.1 predicted the next-year size of telemetry territories better than a constant in validation (RMSE 298 against 426 km²), and the relaxation of Eq. 8b explained 91% of its variance.

Table 3. Accuracy of the sub-models and process equations against their own data (training 1999–2015; validation 2016–2024). Details in Sections S3–S12.

Equation	Target data	Training	Validation
Eq. 1c, random forest, roe deer	Relative harvest index per grid-year	R^2 0.67, RMSE 0.142 (out-of-fold)	R^2 0.77, RMSE 0.115
Eq. 1b, beta regression, roe deer	as above	R^2 0.46, RMSE 0.181	R^2 0.40, RMSE 0.186
Eq. 1c, random forest, moose calves	as above	R^2 0.71, RMSE 0.126	R^2 0.79, RMSE 0.098
Eq. 1b, beta regression, moose calves	as above	R^2 0.67, RMSE 0.133	R^2 0.49, RMSE 0.153
Eq. 2, habitat suitability H	Territory presence per grid-year	AUC 0.815 [0.799–0.834], TSS 0.50	AUC 0.846–0.861 (five SSPs)
Eq. 3, recruitment	Published benchmarks	Kill rate within the observed range in 100% of pack-years (mean +37%); first-winter survival 0.65 (benchmark 0.70); 3.28 recruits per pack (3.4)	–
Eq. 4, pack size, annual mean	Register	RMSE 1.07, bias +0.48 wolves	RMSE 0.47, bias −0.02 wolves
Eq. 4.2, dissolution rate	Register	0.189 (observed 0.198)	0.223 (observed 0.254)
Eq. 4.1.1, occurrence of human-caused deaths	Rovbase	AUC 0.80 (occupied cells 0.60)	AUC 0.84 (occupied cells 0.57)
Eq. 4.1.2, national mortality rate	Rovbase	Fitted 1999–2014	2015–2023: 0.097 predicted, 0.097 observed
Eq. 5, inflow of new dispersers	Register	R^2 0.57, obs/pred 1.32	R^2 0.49, obs/pred 0.99
Eq. 6b, floater pool	Register	R^2 0.39, obs/pred 1.64	R^2 0.30, obs/pred 1.02
Eq. 7, territories (one-step)	Register	Territories R^2 0.88	New territories obs/pred 1.04; territories 1.00
Eq. 8.1, target territory size	Telemetry, 100% MCP	RMSE 463 km² (constant 454)	RMSE 298 km² (constant 426); $\rho = 0.74$
Eq. 8b, territory-size update	Telemetry, 100% MCP	R^2 0.72, RMSE 239 km²	R^2 0.91, RMSE 103 km²

3.2. Assumption tests

Snow depth did not improve habitat suitability beyond its geographic proxies: replacing it by latitude and elevation lowered the cross-validated RMSE by 12.7% (Holm-adjusted $p < 0.001$), so A1 was not supported (Table 4). Removing urban land and cropland changed the RMSE by 1.1% ($p = 0.97$), so A2 was not supported as a superiority claim, and both classes were retained for their documented effects on wolf settlement and mortality (Recio et al., 2018; Zimmermann et al., 2014). The Eq. 1 deer index was non-inferior to the observed index as a predictor of habitat suitability (ΔRMSE 0.0%), which supports A3 for its use in projections; the pre-specified bias-stationarity test could not be performed (Section 2.5.2). Removing forest and swamp worsened the RMSE by 6.4% and changed projected habitat suitability by more than 10% in more than half of the forcing epochs only under SSP3-7.0, so A4 was flagged as sensitive under that pathway. Treating the reindeer-husbandry area as suitable (A5) increased territories in 2060 from 83 to 87 and moved the centroid 1.3° north (Section 3.7).

Table 4. Assumption tests (Eq. 2; blocked cross-validation, 10 pseudo-absence draws × 5 folds; $\Delta\text{RMSE} = 100 \times (\text{RMSE}_{\text{ref}} - \text{RMSE}_{\text{focal}})/\text{RMSE}_{\text{ref}}$, positive when the focal variant is better; Holm correction across A1–A3).

ID	Comparison (focal vs reference)	Test	RMSE ref / focal	ΔRMSE %	p_{Holm}	Decision
A1	Snow depth vs latitude and elevation	Superiority	0.395 / 0.437	−12.7	< 0.001	Not supported
A2	Full land cover vs without urban and cropland	Superiority	0.437 / 0.437	−1.1	0.97	Not supported
A3	Eq. 1 deer index vs observed index	Non-inferiority	0.439 / 0.437	0.0	0.42	Supported
A4	With vs without forest and swamp	Covariate removal	0.459 / 0.437	+6.4	< 0.001	Sensitive under SSP3-7.0
A5	Reindeer-husbandry area unsuitable vs suitable	Sensitivity run	–	–	–	Territories 2060: 83 vs 87; centroid 57.6 vs 58.9 °N

3.3. Historical validation

The free run reproduced the colonisation of 1999–2015 (Figure 2, Table 5). Territories rose from 10 to 67 against 70 observed ($R^2 = 0.90$), pack wolves were reproduced without bias ($R^2 = 0.92$, observed/predicted 0.99), and the floater pool was matched in training ($R^2 = 0.83$). Out of sample, the model reproduced the levelling of 2016–2024, which arises from Eq. 4.1.2 calibrated on 1999–2014: territories in 2024 were 84 (95% of replicates 68–100) against 76 observed, pack wolves 323 against 287, and the mean annual foundings and losses (19.2 and 17.3 territories yr^{-1}) matched the register (19.6 and 18.9). The occupied range was reproduced in extent (45 against 38 grids in 2024) and in position (grid-year occupancy AUC 0.91 in training and 0.85 in validation; cell-mean territory count $r = 0.69$ and 0.50), and the density-weighted centroid in 2024 was 59.0 against 59.1 °N. Floaters were under-predicted in validation (observed/predicted 1.18), and mean territory size was 17–20% below the register, whose sizes are 93% imputed from latitude, whereas the telemetry sizes were reproduced (Table 3). Territorial wolf density

was therefore over-predicted (observed/predicted 0.78 in training and 0.88 in validation), and its year-to-year fluctuations were not reproduced. Started each year from the observed state, the one-step prediction reproduced territories (observed/predicted 1.15 and 1.11), pack wolves (0.94 and 1.01) and floaters (1.10 and 0.93) and placed territories in the right cells (r = 0.78 and 0.85).

Table 5. Validation of the coupled model against the register (free run; replicate mean, validation as the mean of the five SSPs; obs/pred = ratio of observed to predicted totals).

Variable	Training 2000–2015: R^2 / RMSE / obs/pred	Validation 2016–2024: R^2 / RMSE / obs/pred	2015: observed / model	2024: observed / model (95%)
Territories	0.90 / 6.1 / 1.12	0.21 / 5.7 / 0.96	70 / 67	76 / 84 (68–100)
Pack wolves	0.92 / 21.9 / 0.99	0.20 / 30.7 / 0.98	303 / 259	287 / 323 (261–384)
Floaters	0.83 / 16.4 / 0.99	−0.94 / 29.6 / 1.18	152 / 118	154 / 131 (99–160)
Occupied grids	0.26 / 6.8 / 1.32	−3.17 / 5.3 / 0.89	33 / 35	38 / 45 (36–54)
Mean territory size (km²)[1]	– / 209 / 1.25	– / 162 / 1.20	939 / 768	835 / 768 (714–821)
Territorial density $\tilde{D}$ (wolves per 1,000 km²)	– / 1.3 / 0.78	– / 0.65 / 0.88	4.54 / 4.82	4.69 / 4.83 (4.43–5.28)
Heterogeneity CV_{WD}	– / 0.17 / 1.27	– / 0.04 / 0.96	0.42 / 0.46	0.41 / 0.46 (0.36–0.55)
Centroid C (°N)	– / 0.33 / 1.00	– / 0.62 / 1.01	60.2 / 59.7	59.1 / 59.0 (58.4–59.6)
New / lost territories (yr^{-1})	observed 11.1 / 7.3; model 9.5 / 6.0	observed 19.6 / 18.9; model 19.2 / 17.3	–	–
Grid-year occupancy AUC; cell-mean territories r	0.91; 0.69	0.85; 0.50	–	–

[1] Register sizes, 93% imputed from latitude; R^2 not shown where the observed series has little variance around a trend ($R^2 < -1$).

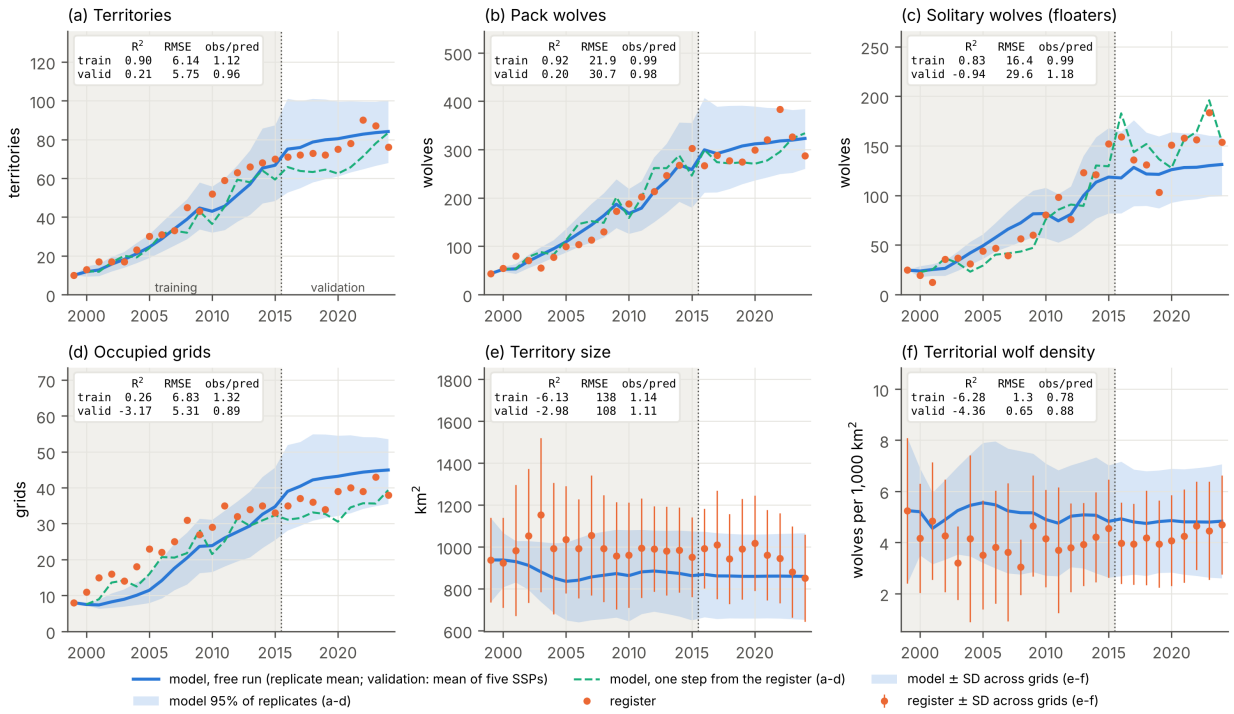


Figure 2. Validation of the coupled model against the register, 1999–2024: (a) territories, (b) pack wolves, (c) solitary wolves, (d) occupied grids, (e) territory size per occupied grid and (f) territorial wolf density per occupied grid. Lines show the replicate mean of the free run from the 1999 register (500 replicates per SSP; validation 2016–2024 as the mean of the five SSPs), shades its 95% replicate range (a–d) or ± SD across grids (e–f), and dashed lines the one-step prediction from the observed state of the previous winter (a–d); dots show the register, with ± SD across grids (e–f). Training 2000–2015 is shaded; accuracy metrics are given top-left.

3.4. Sensitivity analysis: module-level PRCC

Of the 200 Latin-hypercube parameter sets, 10% led to the collapse of the population before 2060, and the remainder gave 2–204 territories in 2060 (median 76; Figure 3). The number of territories was governed by the Pack Module: the scale of human-caused mortality (PRCC = −0.85), the inbreeding-depression slope (−0.78), the non-food survival of pups (+0.73), the life expectancy (+0.73) and fecundity (+0.57), together with the pairing probability of the Territory Module (+0.65) and the dispersal parameters ($Age_{dispersal}$ −0.55, disprate +0.47). The Habitat Module had little influence: a ±20% scaling of deer availability had a PRCC of +0.24 and that of habitat suitability none that was significant. Territorial density and its heterogeneity in 2060 depended on the same demographic parameters and, in addition, on the territory-size parameters of the Territory Module (S_{min} −0.49 on $\bar{D}$; $\bar{S}$ +0.68 and S_{min} −0.64 on CV_{WD}), which barely affected the number of territories. The slope of the H1 estimand was positive in 77% of the non-collapsed parameter sets and decreased with the inbreeding-depression slope (PRCC = −0.63) and S_{min} (−0.45); the slope of the H2 estimand was positive in 82% and decreased mainly with human-caused mortality (−0.52).

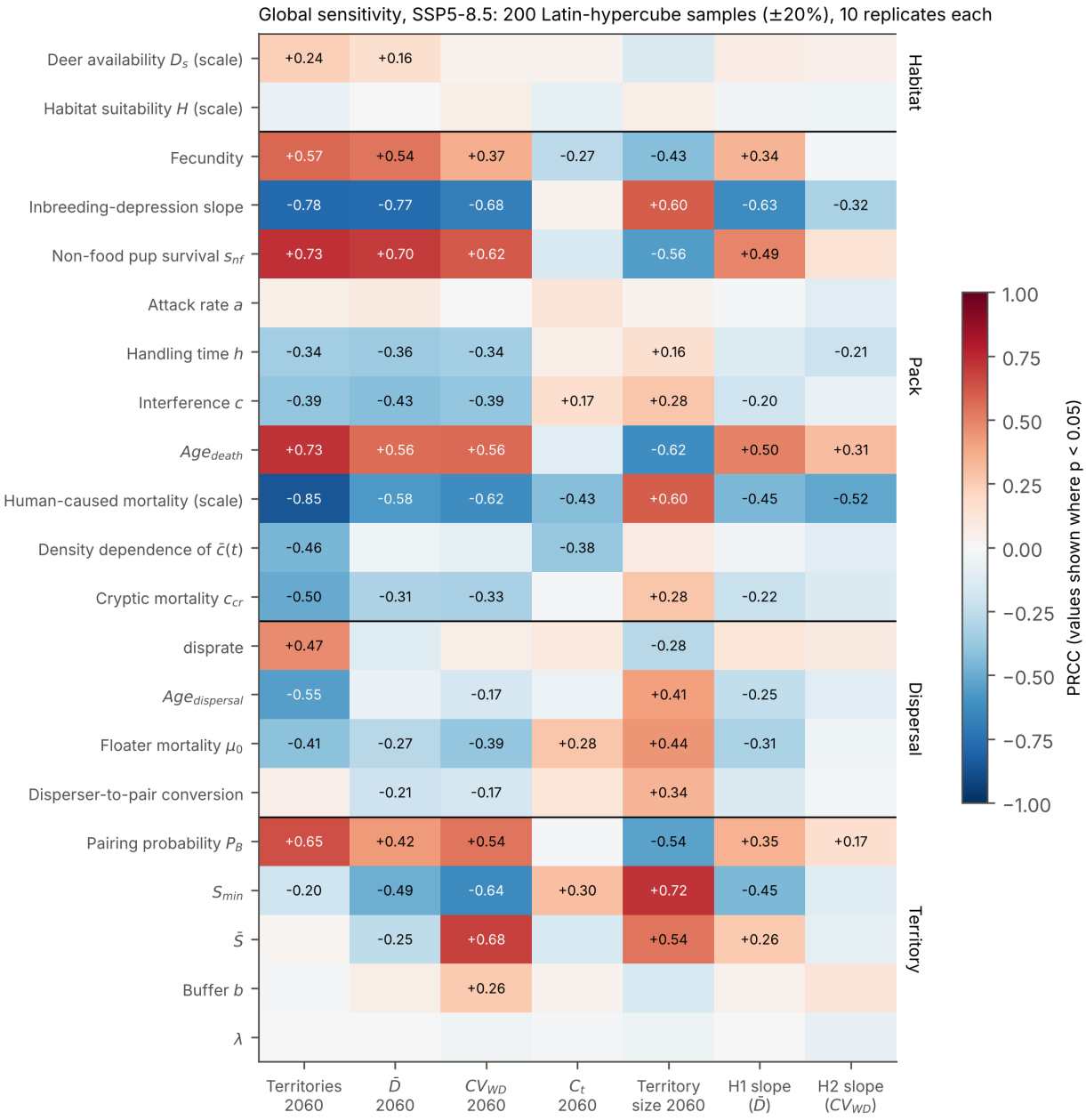


Figure 3. Global sensitivity of the coupled model (SSP5-8.5): partial rank correlation coefficients (PRCC) between 21 parameters, grouped by module and varied within ±20% by Latin-hypercube sampling (200 samples × 10 replicates), and the 2060 territories, territorial density $\bar{D}$, heterogeneity CV_{WD}, centroid C and mean territory size, and the slopes of the H1 and H2 estimands. Values are shown where $p < 0.05$; samples in which the population collapsed (10%) are excluded.

3.5. Wolf population projections and hypothesis tests

All five SSPs produced concordant trajectories (Figure 4). Territories continued to rise after 2024, peaked at 90–91 around 2040 and declined to 81–84 by 2060, with 95% replicate ranges of 70–95; total wolves peaked at about 490 around 2038 and declined to 407–433. The decline followed the

rise of the inbreeding coefficient from 0.27 in 2024 to 0.32 in 2060, which lowered the inbreeding-depression factor from 0.52 to 0.45, and the density-dependent human-caused mortality of Eq. 4.1.2. Mean territory size fell from 807 km² in the baseline to 596–666 km² in 2060, the occupied range contracted from 45 grids in 2024 to 33–40, and the density-weighted centroid moved south from 59.9 °N (baseline) to 57.6–58.0 °N. The pathways differed little in territories (3% in 2060) and wolves (6%), and more in occupied grids (17%), territorial density (12%) and mean territory size (11%), with the high-emission pathways giving fewer occupied grids, smaller territories and higher densities.

H1 was supported in its first form (H1a, Table 6). Under SSP5-8.5, the epoch-mean territorial density rose from 4.82 to 5.91 wolves per 1,000 km² (slope $+3.05 \times 10^{-5}$ wolves km^{-2} yr^{-1}, 95% CI 2.00–4.10 $\times 10^{-5}$, Holm-adjusted $p < 0.001$), 6.9% above the 1999–2015 baseline over the projection and 15.7% in the last epoch, a total change of 1.28×10^{-3} against an MDE of 0.79×10^{-3}. The slope was positive in all replicates and significant under every pathway, although only marginally under SSP1-1.9 and SSP1-2.6 (Holm-adjusted $p = 0.042$ and 0.043). H2 was not supported under the confirmatory scenario (H2c): heterogeneity rose from 0.43 to about 0.50 within the first three epochs and remained there, 16.7% above the baseline over the projection, but its trend across the eight epochs was not significant (slope $+1.12 \times 10^{-3}$ yr^{-1}, 95% CI -0.18 to 2.41×10^{-3}, Holm-adjusted $p = 0.079$; positive in 83% of replicates) and, at 0.047, well below the MDE of 0.19. Heterogeneity increased significantly only under SSP1-1.9 and SSP1-2.6 (H2b), under which the range contracted less (40 against 33 occupied grids in 2060).

Table 6. Confirmatory trend tests on eight 6-year epoch means, 2016–2060 (two-sided linear trend test, 6 df; Holm–Bonferroni across H1 and H2 within each scenario). SSP5-8.5 is confirmatory; the other pathways are exploratory.

Scenario	H1: slope of $\bar{D}$ (10^{-5} wolves km^{-2} yr^{-1}) [95% CI]	p_{Holm}	Outcome	H2: slope of CV_{WD} (10^{-3} yr^{-1}) [95% CI]	p_{Holm}	Outcome
SSP1-1.9	1.36 [0.07, 2.64]	0.042	H1a	2.03 [1.16, 2.90]	0.003	H2b
SSP1-2.6	1.33 [0.06, 2.60]	0.043	H1a	2.05 [1.13, 2.98]	0.003	H2b
SSP2-4.5	1.83 [0.91, 2.76]	0.006	H1a	0.94 [−0.41, 2.29]	0.14	H2c
SSP3-7.0	2.28 [1.05, 3.51]	0.008	H1a	1.16 [−0.13, 2.45]	0.069	H2c
SSP5-8.5	**3.05 [2.00, 4.10]**	**< 0.001**	**H1a**	**1.12 [−0.18, 2.41]**	**0.079**	**H2c**

Supporting evidence under SSP5-8.5. H1: baseline (1999–2015) 5.11 wolves per 1,000 km²; projection mean +6.9%; last epoch +15.7%; positive slope in 100% of replicates; Mann–Kendall $p = 0.002$. H2: baseline 0.416; projection mean +16.7%; last epoch +18.9%; positive slope in 83% of replicates; Mann–Kendall $p = 0.54$.

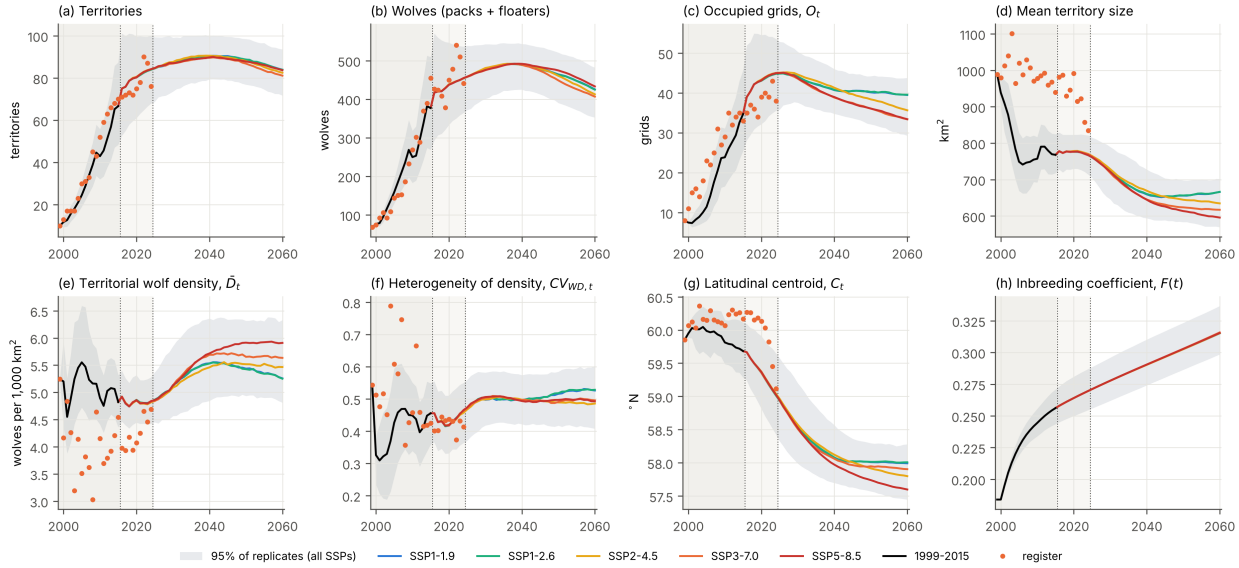


Figure 4. Projections 1999–2060 under five SSPs: (a) territories, (b) wolves, (c) occupied grids, (d) mean territory size, (e) territorial wolf density $\bar{D}_t$, (f) its heterogeneity $CV_{WD,t}$, (g) density-weighted latitudinal centroid C_t and (h) inbreeding coefficient F(t). Lines are replicate means (500 replicates per SSP; black: 1999–2015, common forcing), the grey shade is the 95% range of all replicates, and dots are the register. Training and validation periods are shaded.

3.6. Spatial regime structure

The model kept the occupied range within its observed footprint until 2024 (Figure 5) but distributed it differently: in 2024, 48% of simulated territories lay south of 59 °N against 22% in the register, and 50% between 59 and 62 °N against 75%. After 2024 this southward redistribution continued. By 2060, 78% (SSP1-2.6) to 87% (SSP5-8.5) of territories lay south of 59 °N, 11–19% between 59 and 62 °N and 2–3% north of 62 °N, and territories were concentrated in southern Sweden at up to five per grid. The redistribution follows the mortality pattern: P(g,t) averaged 0.49 in the grids at 59–62 °N, the core of the observed range, against 0.19 south of 58 °N, so the predicted human-caused mortality of a territory south of 58 °N is less than half that in the core. With a spatially uniform mortality pattern, the centroid remained at 59.2 °N in 2060 (Section 3.7).

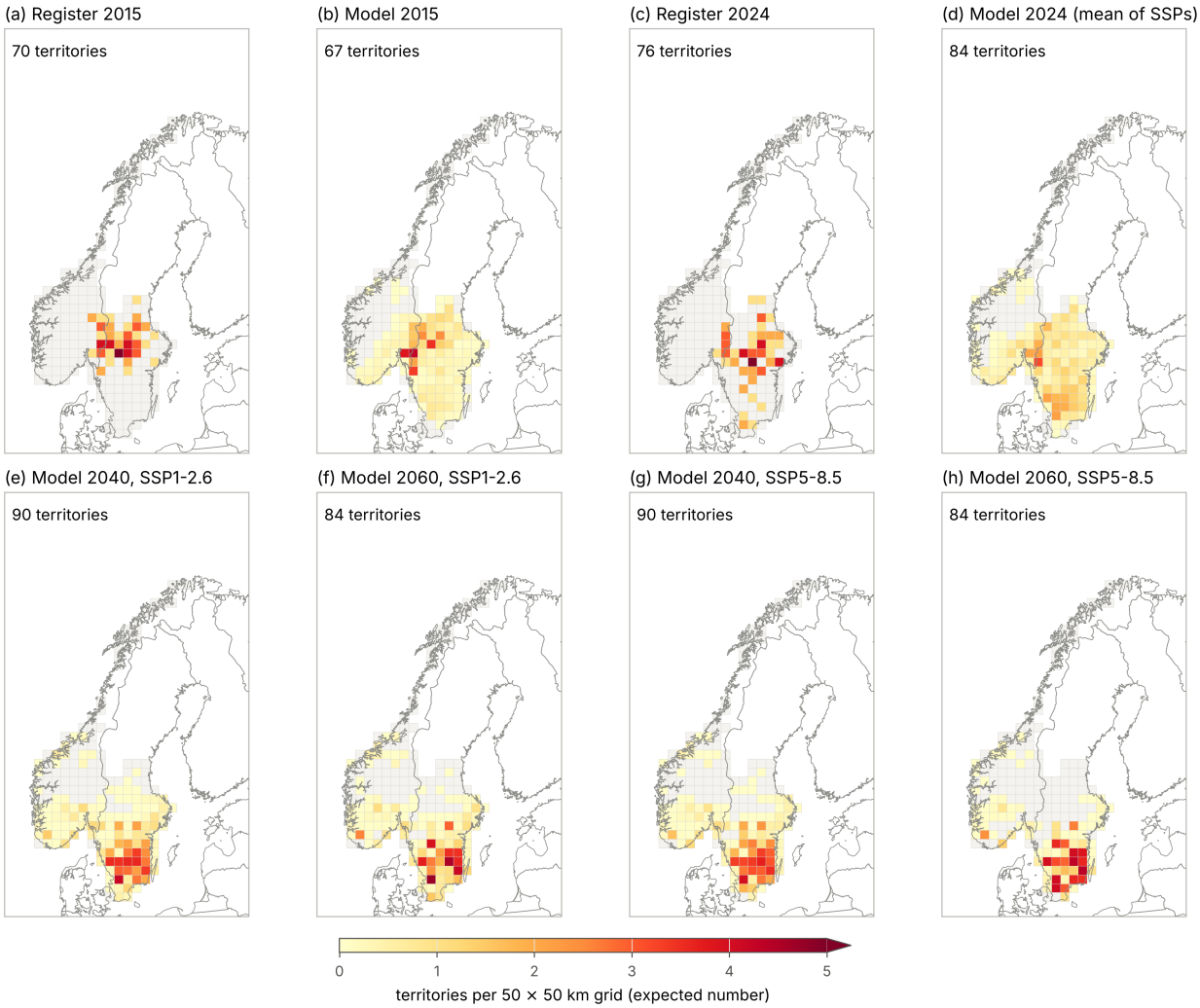


Figure 5. Expected number of territories per 50 × 50 km grid: (a) register 2015, (b) model 2015, (c) register 2024, (d) model 2024 (mean of the five SSPs), (e–f) model 2040 and 2060 under SSP1-2.6, (g–h) model 2040 and 2060 under SSP5-8.5 (replicate means). Grey cells are the model domain; cells inside the reindeer-husbandry area and Svalbard are excluded. Basemap: Natural Earth 10 m countries; ETRS89/LAEA Europe (EPSG:3035).

3.7. Sensitivity analysis

In the OAT analysis (Figure 6), territories in 2060 (baseline 83) responded most to the scale of human-caused mortality (47–125 for +20% and −20%), the inbreeding-depression slope (42–97), the non-food survival of pups (46–99), the life expectancy (50–101), the pairing probability (52–104), fecundity (51–90), the density dependence of the national mortality rate (69–103), the dispersal parameters (64–97) and cryptic mortality (70–95), and least to the territory-size parameters (79–88). Territorial density in 2060 (baseline 5.9 wolves per 1,000 km²) ranged from 4.2 to 6.8 and its heterogeneity from 0.42 to 0.55, with S_{min} and $\bar{S}$ shifting density and heterogeneity at nearly constant territory counts. The factorial analyses widened these ranges ($P_B \times \mu_0$: 37–112 territories; a × h: 55–88; $\bar{S} \times \lambda$: 83–84). The H1 slope remained positive in all OAT runs except

for a 20% steeper inbreeding-depression slope, under which it was zero, and it was negative for a conversion factor of 0.3. A conversion factor of 0.3 reduced territories in 2060 to 40 and that of 0.65 to 70, and a ±20% change in the initial territory count changed territories in 2024 by −13% to +10% and in 2060 by −9% to +5%, exceeding the 10% criterion only in the validation period. Treating the reindeer-husbandry area as suitable (A5) gave 87 territories and a centroid of 58.9 °N in 2060.

Among the structural alternatives, the mortality formulation dominated. Rovbase rates to 2024 gave 110 territories in 2024 against 76 observed, because the rates realised by a population held near 75 territories are applied to a larger simulated population; followed by the constant 1999–2024 mean rate, the population kept growing to 172 territories in 2060, whereas followed by Eq. 4.1.2 it converged to the baseline (85 territories). A spatially uniform mortality pattern kept the centroid at 59.2 °N, lowered territorial density to 4.5 wolves per 1,000 km² and heterogeneity to 0.31 in 2060, and reversed the signs of both confirmatory slopes. The buffered space for new territories gave 93 territories, smaller territories (439 km²) and higher density (8.0 wolves per 1,000 km²) and heterogeneity (0.61) in 2060. Freezing the inbreeding coefficient from 2025 gave 93 territories and 524 wolves in 2060, without husbandry inflation 86 territories, and the rebuilt mortality pattern 84 territories. The deer index projected from 2016 instead of the observed index to 2024 changed all outputs by less than 1%. No run met the instability criterion.

The input bounds of deer availability and habitat suitability gave 69–86 territories in 2060 (Section 2.5.4). The H1 slope was positive at every bound (2.2–3.0 × 10^{-5} wolves km^{-2} yr^{-1}) and the H2 slope as well (0.4–1.3 × 10^{-3} yr^{-1}), so neither verdict was inconclusive.

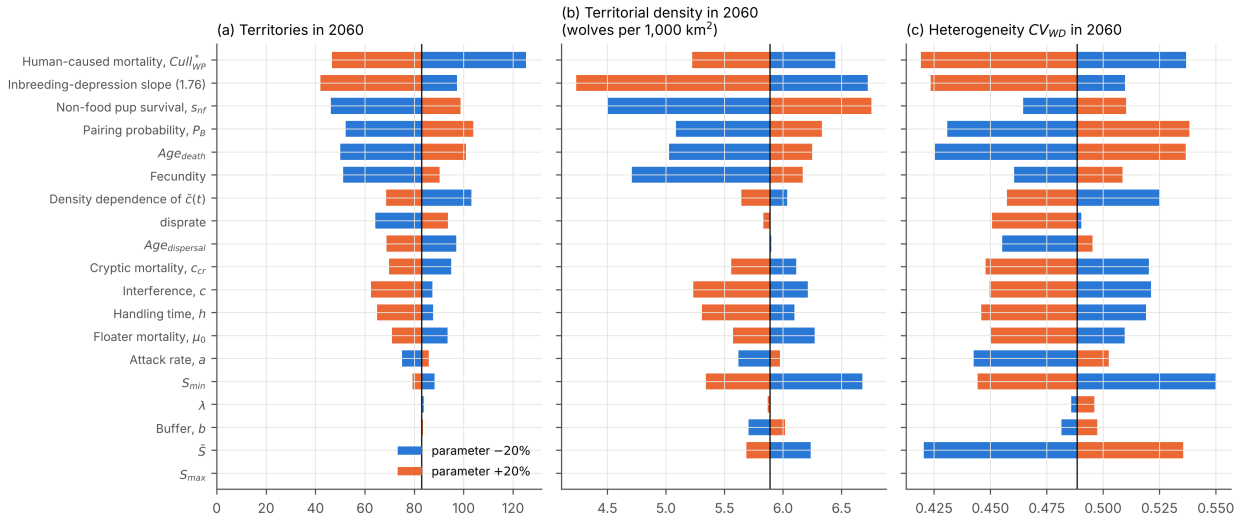


Figure 6. One-at-a-time sensitivity (±20%, SSP5-8.5, 100 replicates) of (a) territories, (b) territorial wolf density and (c) heterogeneity CV_{WD} in 2060. Bars show the change from the baseline (vertical line) for a 20% decrease (blue) and increase (orange) of each parameter, ordered by their effect on territories.

3.8. Regime shift detection

The first principal component of the standardised regime vector explained 65–68% of its variance, loading positively on territorial density, occupied grids and heterogeneity and negatively on the centroid (Figure 7). STARS (cut-off 5 years) detected four shifts under SSP5-8.5 and SSP3-7.0 (2004, 2014, 2023 and 2028), four under SSP1-1.9 and SSP1-2.6 (2004, 2021, 2026 and 2034–2035) and three under SSP2-4.5 (2004, 2022 and 2027). Under SSP5-8.5, the regimes moved from a small core (1999–2003; 8 occupied grids, centroid 60.0 °N) through colonisation (2004–2013; 20 grids) and the filling of the range (2014–2022; 40 grids, 59.5 °N) to a short transition (2023–2027; 45 grids, 58.9 °N) and a final regime from 2028 to 2060 with fewer occupied grids (38), a southern centroid (58.0 °N) and higher and more heterogeneous densities (5.7 wolves per 1,000 km²; CV 0.50). Within-regime variability declined from 1.57 in the first to 0.28 in the transition regime and was 0.69 in the final regime. Across replicates, the median number of shifts was 4 (5–95%: 3–5), and the final regime persisted for a median of 24–30 years. Cut-off lengths of 3–7 years detected three to four shifts, always including the colonisation shift around 2005 and one or two projection-period shifts between 2021 and 2036. These results are exploratory and do not alter the confirmatory decisions.

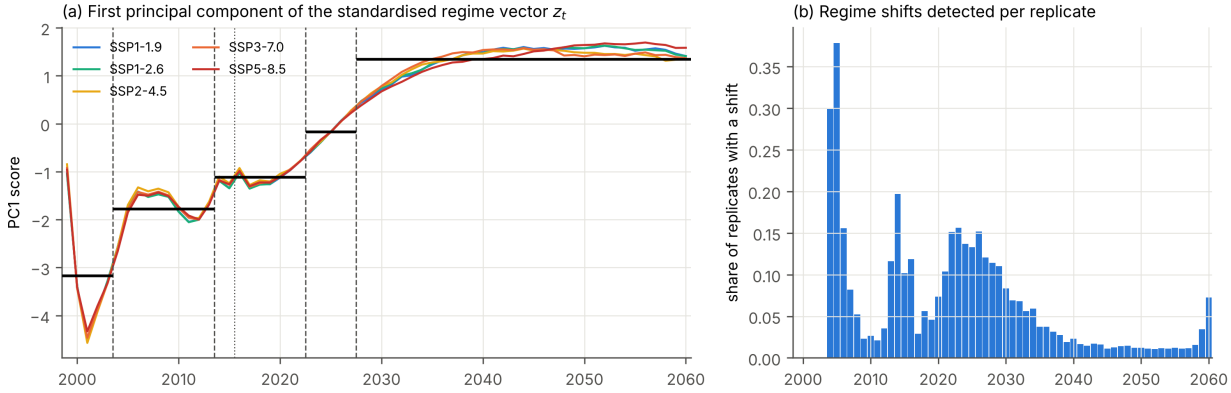


Figure 7. Regime shifts in the territorial wolf regime. (a) First principal component of the standardised regime vector $z_t = (C_t, \bar{D}_t, O_t, CV_{WD,t})$ for the replicate means of the five SSPs; horizontal bars show the regime means and dashed lines the shifts detected by STARS (cut-off 5 years) under SSP5-8.5. (b) Share of the 2,500 replicates (500 per SSP) with a shift detected in each year.

4. Discussion

This study coupled machine-learning estimators of deer availability, habitat suitability and the spatial pattern of human-caused mortality with a deterministic pack-level model and projected Scandinavian wolf territories under five SSPs to 2060. Without parameters fitted to the coupled trajectory, the model reproduced the colonisation of 1999–2015 and, out of sample, the levelling of the population after 2015. Under all pathways, territories peaked at about 90 around 2040 and declined slightly to 2060, territorial density increased (H1a), and its heterogeneity rose to a higher level within the first decade but did not trend under the confirmatory scenario (H2c). The

pathways differed little, and both the increase in density and the southward shift of the range depended on the spatial pattern of human-caused mortality.

4.1. Model performance and predictive architecture

The sub-models separate where wolves can settle from how many they become. Habitat suitability discriminated occupied from unoccupied cells (AUC 0.82 in cross-validation, 0.85–0.86 in validation), but territory size did not decrease with it: telemetry territories were larger where suitability was higher, and every suitability-based size rule predicted worse than a constant. We therefore let suitability govern where territories form and let the space left by neighbours govern their size, which the telemetry supports (Eq. 8.1 validation RMSE 298 against 426 km² for a constant) and which agrees with mechanistic territory models in which size emerges from the spacing of neighbours as much as from resources (Moorcroft et al., 2006; Sells & Mitchell, 2020). The demographic equations reproduced their own processes with literature parameters only, so the coupled behaviour is not the product of compensating calibrations. The weakest link is the mortality pattern: P(g,t) locates human-caused deaths well over time (AUC 0.80–0.84) but ranks the risk among occupied cells only weakly (0.57–0.60), because deaths can only be recorded where wolves live. Its spatial contrast therefore partly reflects the historical range itself. Spatial capture–recapture analyses of the same population show that about two-thirds of wolf deaths remain undetected and that the risk of legal killing increases with local wolf density (Milleret et al., 2025), so recorded deaths are a biased map of risk, a limitation we return to in Section 4.7.

4.2. Historical validation and spatial allocation

The national trajectory was reproduced in both phases of the recovery. The colonisation phase (R^2 0.90 for territories, 0.92 for pack wolves) emerged from recruitment, dispersal and pairing with literature parameters, and the plateau of 2016–2024 emerged from the density dependence of human-caused mortality calibrated before it (Eq. 4.1.2). The plateau is the stronger test, because it is a change of regime that the training data did not contain, and the model predicted both its level (84 against 76 territories in 2024) and its turnover (19 foundings and 17 losses per year against 20 and 19). Applying the realised Rovbase rates of 2016–2024 to the simulated population, in contrast, overshot the 2024 count by 45%, because a rate realised by a population held at about 75 territories does not hold a larger one; culling acts as a removal that scales with the population rather than as a fixed rate (Liberg, Chapron, et al., 2012; Milleret et al., 2017). At grid level, the model placed territories in the right part of Scandinavia (occupancy AUC 0.91 and 0.85) but not in the right cells (cell-mean r = 0.69 and 0.50), and by 2024 it had moved half of them south of 59 °N, against a fifth in the register. Territorial density was over-predicted by 12–22% because simulated territories were 17–20% smaller than the register sizes; as 93% of those sizes are imputed from latitude, and the telemetry sizes were reproduced, this bias is partly a property of the observations rather than of the model.

4.3. Sensitivity structure and climate dependence

Both the local and the global analyses ranked the demographic parameters first: human-caused mortality, inbreeding depression, pup survival, life expectancy and pairing probability each changed the 2060 territory count by a factor of about two within ±20%, whereas deer availability and habitat suitability changed it by less than any of them (PRCC +0.24 and not significant). Climate enters the model through snow depth and land cover in Eqs. 1, 2 and 4.1, and the assumption tests weakened this pathway further: snow depth added nothing to habitat suitability beyond latitude and elevation (A1), consistent with snow acting on wolves through prey vulnerability rather than as a habitat filter (Kittle et al., 2017; Sand et al., 2006a). The pathways therefore diverged in where wolves live and how densely (17% in occupied grids, 12% in density) more than in how many there are (3%), and the divergence arose in the spatial outputs, which depend on land cover through habitat suitability and the mortality pattern, rather than in recruitment. Territory-size parameters controlled density and heterogeneity at almost constant territory counts, so the density hypotheses depend on Eq. 8 more than the population size does.

4.4. Interpretation of hypothesis tests

H1a was supported because the population was redistributed into smaller territories rather than because it grew. After the peak around 2040, territories declined while the range contracted from 45 to 33–40 occupied grids and mean territory size fell by 17–26% from the baseline, so the same number of packs occupied less space. This compression is the mechanism of Eq. 8: the range moves south into cells where the predicted human-caused mortality is less than half that in the current core, territories accumulate there faster than they are lost, and the free space of those cells is shared among more packs. The verdict was robust to the input bounds and to most parameters, but not to the mortality pattern: with a spatially uniform pattern, the range stayed in its core and density declined. H1a should therefore be read as conditional on the land-cover pattern of human-caused mortality continuing to differ between the current core and southern Sweden.

H2 was not supported under SSP5-8.5 because heterogeneity changed as a step rather than a trend: it rose from 0.43 to about 0.50 during the southward transition of 2016–2033 and then remained constant, which a linear trend over eight epochs cannot detect, and the test had an MDE of 0.19, four times the change observed. The significant increase under SSP1-1.9 and SSP1-2.6 came from a smaller contraction of the range, which left more lightly occupied cells beside the dense southern cluster. The step and the regime analysis agree: the final regime, from 2028 under SSP5-8.5, combines a southern centroid, fewer occupied grids and higher, more heterogeneous densities, and it persisted to 2060 in most replicates. Because the model has no feedback from wolves on prey or vegetation, these regimes are forcing-driven modes of spatial organisation, not alternative stable states (Scheffer & Carpenter, 2003).

4.5. Comparison with prior work

The simulated plateau of 75–90 territories agrees with the stabilisation of the register at 70–90 territories under licensed hunting since 2015 (Wabakken et al., 2026), and the dependence of

territory numbers on human-caused mortality agrees with Liberg, Chapron, et al. (2012), who showed that cryptic poaching slowed the growth of the population. The decline of the inbreeding-depression factor from 0.59 in the baseline to 0.45 in 2060 reproduces, through Eq. 3.1, the consequences of the small effective size of an isolated population (Liberg et al., 2005; Laikre et al., 2016), and it is the main reason why territory numbers fall after 2040. Smaller territories in the south agree in direction with the latitudinal gradient of territory size reported by Mattisson et al. (2013), although in the model they arise from compression rather than from latitude or prey. The southward shift contrasts with an agent-based model of the Scandinavian recolonisation, in which low rates of territory termination drove the expansion and wolves did not colonise southern Sweden by 2030 (Recio et al., 2020); in our model, the land-cover pattern of human-caused mortality makes southern Sweden the part of the range where territories are lost most slowly. The primacy of mortality agrees with a spatially explicit individual-based model of Iberian wolves, in which the mortality of resident wolves, not of dispersers, determined range dynamics (Morales-González et al., 2026). Compared with individual-based recolonisation models with fixed habitat (Marucco & McIntire, 2010), the pack-level formulation trades individual detail for the ability to propagate land-use and climate scenarios through habitat suitability, prey and mortality over the whole of Scandinavia.

4.6. Conservation and management implications

Under the continuation of the current density-dependent mortality, the model projects a population that remains at 80–90 territories to 2060 regardless of the climate pathway, so management policy, not climate, sets the size of the population over this horizon. Two processes nevertheless change its structure. First, inbreeding continues to rise and lowers the litter retained under inbreeding by a quarter relative to 1999–2015, so the long-term status of the population depends on gene flow from the Finnish–Russian population, which the model does not include (Laikre et al., 2016). Second, the range may shift south, where wolves would live at higher density in smaller territories and closer to agricultural and settled landscapes; this shift is the least certain projection of the model, because it rests on the land-cover pattern of human-caused mortality, but if it occurs it would move conflicts with livestock and hunting interests into new areas.

4.7. Limitations

Several constraints bound these projections. The mortality pattern P(g,t) was learned from where deaths were recorded, which is also where wolves lived, so part of its contrast between the core and the south may reflect exposure rather than risk; the southward shift and H1a depend on it, and the uniform pattern reverses both. The model has no immigration, no feedback on prey, and no explicit management rule beyond the density dependence of the national mortality rate, so it cannot represent quotas, zoning or changes in policy. The 50 × 50 km grid cannot resolve territory boundaries or dispersal corridors, and the planned comparison with a 25 × 25 km grid was not carried out. Register territory sizes are largely imputed, so the territory-size and density components of the validation rest on 90 telemetry pack-years. Floaters were under-predicted after 2015, and the initial territory count affected the 2024 projection by up to 13%. The A3

bias-stationarity test could not be performed, and the prediction uncertainty of deer availability and habitat suitability was bounded rather than propagated. Semi-domestic reindeer husbandry, and the policy that keeps wolves out of it, were assumed to persist, although the husbandry area offers abundant prey (A5). Finally, species–environment relationships were assumed stationary over 60 years (Elith & Leathwick, 2009).

4.8. Future directions

Three extensions follow from these limitations. First, replacing the occurrence of recorded deaths by spatially explicit estimates of cause-specific mortality risk from open-population spatial capture–recapture models (Milleret et al., 2025) would separate risk from exposure and test the southward shift. Second, coupling the model with an explicit management module (quotas, zones and their decision rules) and with immigration from Finland and Russia would allow policy and genetic scenarios to be compared with the SSP pathways explored here. Third, a finer grid with telemetry-based dispersal and territory sizes, and a formal Bayesian calibration that propagates the uncertainty of the sub-models (Hartig et al., 2011), would improve the spatial allocation and quantify the confidence in the regime projections.

Acknowledgements

We thank the Norwegian and Swedish large-carnivore monitoring programmes (Rovdata and the SLU Wildlife Damage Centre) and the SKANDULV project for the monitoring and telemetry data, Viltdata, Statistics Norway and Hjorteviltregisteret for the harvest statistics, and the providers of LUCAS LUC, ERA5-Land and the CMIP6 EC-Earth3-Veg-LR projections.

Author contributions

[To be confirmed by the authors.] Sinchan Ghosh: conceptualisation, methodology, software, formal analysis, visualisation, writing – original draft. Oskar Franklin: conceptualisation, methodology, supervision, writing – review and editing. Barbara Zimmermann: data curation, methodology, writing – review and editing.

Funding

[To be completed by the authors.]

Competing interests

The authors declare no competing interests.

Use of generative AI

The authors used Claude (Anthropic) to reconstruct and document the model code from the authors' equation scripts, to run the simulations and analyses specified by the authors, and to draft and edit parts of the text. All model decisions were made by the authors, who checked the code, results and text and take full responsibility for the content.

Data and code availability

The model code (`model.py` and the scripts of each equation), the analysis and figure scripts, the processed inputs and the simulation outputs are available at https://github.com/gsinchanpostdoc/Wolf-model and will be archived on Zenodo with a DOI. The monitoring records and dead-wolf records are available from Rovbase (https://rovbase.no) and the national monitoring reports, and the land-cover, snow and harvest data from the sources given in Section 2.1. The Supplementary Information contains the parameter table (Table S1), the processing of the input data, the fitting and validation of every equation, and the full results of the validation, projections, hypothesis tests, regime analysis and sensitivity analyses.

References

Åkesson, M., Liberg, O., Sand, H., Wabakken, P., Bensch, S., & Flagstad, Ø. (2016). Genetic rescue in a severely inbred wolf population. *Molecular Ecology, 25*(19), 4745–4756. https://doi.org/10.1111/mec.13797

Åkesson, M., Svensson, L., Flagstad, Ø., Wabakken, P., & Frank, J. (2022). Wolf monitoring in Scandinavia: Evaluating counts of packs and reproduction events. *Journal of Wildlife Management, 86*(4), e22206. https://doi.org/10.1002/jwmg.22206

Axnér, E., Cederlund, E., Ågren, E. O., & Dalin, A.-M. (2023). Characteristics of reproductive organs and reproductive potential in Scandinavian female grey wolves (*Canis lupus*). *Animal Reproduction Science, 255*, 107266. https://doi.org/10.1016/j.anireprosci.2023.107266

Barbet-Massin, M., Jiguet, F., Albert, C. H., & Thuiller, W. (2012). Selecting pseudo-absences for species distribution models: How, where and how many? *Methods in Ecology and Evolution, 3*(2), 327–338. https://doi.org/10.1111/j.2041-210X.2011.00172.x

Bergqvist, G., Wallgren, M., Jernelid, H., & Bergström, R. (2018). Forage availability and moose winter browsing in forest landscapes. *Forest Ecology and Management, 419–420*, 170–178. https://doi.org/10.1016/j.foreco.2018.03.048

Bischof, R., Milleret, C., Dupont, P., Chipperfield, J., Tourani, M., Ordiz, A., de Valpine, P., Turek, D., Royle, J. A., Gimenez, O., Flagstad, Ø., Åkesson, M., Svensson, L., Brøseth, H., & Kindberg, J. (2020). Estimating and forecasting spatial population dynamics of apex predators using transnational genetic monitoring. *Proceedings of the National Academy of Sciences, 117*(48), 30531–30538. https://doi.org/10.1073/pnas.2011383117

Caswell, H. (2001). *Matrix population models: Construction, analysis, and interpretation* (2nd ed.). Sinauer Associates.

Chapron, G., Wikenros, C., Liberg, O., Wabakken, P., Flagstad, Ø., Milleret, C., Månsson, J., Svensson, L., Zimmermann, B., Åkesson, M., & Sand, H. (2016). Estimating wolf (*Canis lupus*) population size from number of packs and an individual based model. *Ecological Modelling, 339*, 33–44. https://doi.org/10.1016/j.ecolmodel.2016.08.012

Donohue, I., Petchey, O. L., Montoya, J. M., Jackson, A. L., McNally, L., Viana, M., Healy, K., Lurgi, M., O'Connor, N. E., & Emmerson, M. C. (2013). On the dimensionality of ecological stability. *Ecology Letters, 16*(4), 421–429. https://doi.org/10.1111/ele.12086

Dormann, C. F., Elith, J., Bacher, S., Buchmann, C., Carl, G., Carré, G., … Lautenbach, S. (2013). Collinearity: A review of methods to deal with it and a simulation study evaluating their performance. *Ecography, 36*(1), 27–46. https://doi.org/10.1111/j.1600-0587.2012.07348.x

Döscher, R., Acosta, M., Alessandri, A., Anthoni, P., Arsouze, T., Bergman, T., … Zhang, Q. (2022). The EC-Earth3 Earth system model for the Coupled Model Intercomparison Project 6. *Geoscientific Model Development, 15*(7), 2973–3020. https://doi.org/10.5194/gmd-15-2973-2022

Eberhardt, L. L. (2002). A paradigm for population analysis of long-lived vertebrates. *Ecology, 83*(10), 2841–2854. https://doi.org/10.1890/0012-9658(2002)083[2841:APFPAO]2.0.CO;2

Elith, J., & Leathwick, J. R. (2009). Species distribution models: Ecological explanation and prediction across space and time. *Annual Review of Ecology, Evolution, and Systematics, 40*, 677–697. https://doi.org/10.1146/annurev.ecolsys.110308.120159

Elith, J., Leathwick, J. R., & Hastie, T. (2008). A working guide to boosted regression trees. *Journal of Animal Ecology, 77*(4), 802–813. https://doi.org/10.1111/j.1365-2656.2008.01390.x

Eriksson, M., & Dalerum, F. (2018). Identifying potential areas for an expanding wolf population in Sweden. *Biological Conservation, 220*, 170–181. https://doi.org/10.1016/j.biocon.2018.02.019

Ferrari, S., & Cribari-Neto, F. (2004). Beta regression for modelling rates and proportions. *Journal of Applied Statistics, 31*(7), 799–815. https://doi.org/10.1080/0266476042000214501

Frankham, R. (1995). Effective population size/adult population size ratios in wildlife: A review. *Genetical Research, 66*(2), 95–107. https://doi.org/10.1017/S0016672300034455

Gaston, K. J., Blackburn, T. M., Greenwood, J. J. D., Gregory, R. D., Quinn, R. M., & Lawton, J. H. (2000). Abundance–occupancy relationships. *Journal of Applied Ecology, 37*(Suppl. 1), 39–59. https://doi.org/10.1046/j.1365-2664.2000.00485.x

Gervasi, V., Sand, H., Zimmermann, B., Mattisson, J., Wabakken, P., & Linnell, J. D. C. (2013). Decomposing risk: Landscape structure and wolf behavior generate different predation patterns in two sympatric ungulates. *Ecological Applications, 23*(7), 1722–1734. https://doi.org/10.1890/12-1615.1

Grilo, C., Lucas, P. M., Fernández-Gil, A., Seara, M., Costa, G., Roque, S., Rio-Maior, H., Nakamura, M., Álvares, F., Petrucci-Fonseca, F., & Revilla, E. (2019). Refuge as major habitat

driver for wolf presence in human-modified landscapes. *Animal Conservation, 22*(1), 59–71. https://doi.org/10.1111/acv.12435

Grimm, V., Revilla, E., Berger, U., Jeltsch, F., Mooij, W. M., Railsback, S. F., Thulke, H.-H., Weiner, J., Wiegand, T., & DeAngelis, D. L. (2005). Pattern-oriented modeling of agent-based complex systems: Lessons from ecology. *Science, 310*(5750), 987–991. https://doi.org/10.1126/science.1116681

Hartig, F., Calabrese, J. M., Reineking, B., Wiegand, T., & Huth, A. (2011). Statistical inference for stochastic simulation models – theory and application. *Ecology Letters, 14*(8), 816–827. https://doi.org/10.1111/j.1461-0248.2011.01640.x

Heisey, D. M., & Fuller, T. K. (1985). Evaluation of survival and cause-specific mortality rates using telemetry data. *Journal of Wildlife Management, 49*(3), 668–674. https://doi.org/10.2307/3801692

Hoffmann, P., Reinhart, V., Rechid, D., de Noblet-Ducoudré, N., Davin, E. L., Asmus, C., Bechtel, B., Böhner, J., Katragkou, E., & Luyssaert, S. (2023). High-resolution land use and land cover dataset for regional climate modelling: Historical and future changes in Europe. *Earth System Science Data, 15*(8), 3819–3852. https://doi.org/10.5194/essd-15-3819-2023

Holm, S. (1979). A simple sequentially rejective multiple test procedure. *Scandinavian Journal of Statistics, 6*(2), 65–70.

Jakeman, A. J., Letcher, R. A., & Norton, J. P. (2006). Ten iterative steps in development and evaluation of environmental models. *Environmental Modelling & Software, 21*(5), 602–614. https://doi.org/10.1016/j.envsoft.2006.01.004

Kittle, A. M., Anderson, M., Avgar, T., Baker, J. A., Brown, G. S., Hagens, J., … Fryxell, J. M. (2017). Landscape-level wolf space use is correlated with prey abundance, ease of mobility, and the distribution of prey habitat. *Ecosphere, 8*(4), e01783. https://doi.org/10.1002/ecs2.1783

Kojola, I., Aspi, J., Hakala, A., Heikkinen, S., Ilmoni, C., & Ronkainen, S. (2006). Dispersal in an expanding wolf population in Finland. *Journal of Mammalogy, 87*(2), 281–286. https://doi.org/10.1644/05-MAMM-A-061R2.1

Laikre, L., Olsson, F., Jansson, E., Hössjer, O., & Ryman, N. (2016). Metapopulation effective size and conservation genetic goals for the Fennoscandian wolf (*Canis lupus*) population. *Heredity, 117*(4), 279–289. https://doi.org/10.1038/hdy.2016.44

Ledder, G., Homp, M. R., & Rinaldi, S. (2021). A discrete/continuous time resource competition model and its implications. *Journal of Biological Dynamics, 15*(Suppl. 1), 18–37. https://doi.org/10.1080/17513758.2020.1862927

Lee, J.-S., Filatova, T., Ligmann-Zielinska, A., Hassani-Mahmooei, B., Stonedahl, F., Lorscheid, I., Voinov, A., Polhill, J. G., Sun, Z., & Parker, D. C. (2015). The complexities of agent-based modeling output analysis. *Journal of Artificial Societies and Social Simulation, 18*(4), 4. https://doi.org/10.18564/jasss.2897

Liberg, O., Andrén, H., Pedersen, H.-C., Sand, H., Sejberg, D., Wabakken, P., Åkesson, M., & Bensch, S. (2005). Severe inbreeding depression in a wild wolf (*Canis lupus*) population. *Biology*

Letters, 1(1), 17–20. https://doi.org/10.1098/rsbl.2004.0266

Liberg, O., Aronson, Å., Sand, H., Wabakken, P., Maartmann, E., Svensson, L., & Åkesson, M. (2012). Monitoring of wolves in Scandinavia. *Hystrix, the Italian Journal of Mammalogy, 23*(1), 29–34. https://doi.org/10.4404/hystrix-23.1-4670

Liberg, O., Chapron, G., Wabakken, P., Pedersen, H. C., Hobbs, N. T., & Sand, H. (2012). Shoot, shovel and shut up: Cryptic poaching slows restoration of a large carnivore in Europe. *Proceedings of the Royal Society B, 279*(1730), 910–915. https://doi.org/10.1098/rspb.2011.1275

Marino, S., Hogue, I. B., Ray, C. J., & Kirschner, D. E. (2008). A methodology for performing global uncertainty and sensitivity analysis in systems biology. *Journal of Theoretical Biology, 254*(1), 178–196. https://doi.org/10.1016/j.jtbi.2008.04.011

Marucco, F., & McIntire, E. J. B. (2010). Predicting spatio-temporal recolonization of large carnivore populations and livestock depredation risk: Wolves in the Italian Alps. *Journal of Applied Ecology, 47*(4), 789–798. https://doi.org/10.1111/j.1365-2664.2010.01831.x

Mattisson, J., Sand, H., Wabakken, P., Gervasi, V., Liberg, O., Linnell, J. D. C., Rauset, G. R., & Pedersen, H. C. (2013). Home range size variation in a recovering wolf population: Evaluating the effect of environmental, demographic, and social factors. *Oecologia, 173*(3), 813–825. https://doi.org/10.1007/s00442-013-2668-x

McKay, M. D., Beckman, R. J., & Conover, W. J. (1979). A comparison of three methods for selecting values of input variables in the analysis of output from a computer code. *Technometrics, 21*(2), 239–245. https://doi.org/10.1080/00401706.1979.10489755

Mech, L. D., & Boitani, L. (Eds.). (2003). *Wolves: Behavior, ecology, and conservation*. University of Chicago Press.

Milleret, C., Dupont, P., Åkesson, M., Brøseth, H., Svensson, L., Kindberg, J., & Bischof, R. (2022). *Estimates of wolf density, abundance, and population dynamics in Scandinavia, 2013–2022* (MINA fagrapport 77). Norwegian University of Life Sciences.

Milleret, C., Dupont, P., Dey, S., Brøseth, H., Kindberg, J., Turek, D., de Valpine, P., Åkesson, M., Wabakken, P., Zimmermann, B., & Bischof, R. (2025). Map of death: Spatially explicit mortality of the grey wolf. *Proceedings of the Royal Society B, 292*(2053), 20250948. https://doi.org/10.1098/rspb.2025.0948

Milleret, C., Wabakken, P., Liberg, O., Åkesson, M., Flagstad, Ø., Andreassen, H. P., & Sand, H. (2017). Let's stay together? Intrinsic and extrinsic factors involved in pair bond dissolution in a recolonizing wolf population. *Journal of Animal Ecology, 86*(1), 43–54. https://doi.org/10.1111/1365-2656.12587

Mitchell, M. S., & Powell, R. A. (2004). A mechanistic home range model for optimal use of spatially distributed resources. *Ecological Modelling, 177*(1–2), 209–232. https://doi.org/10.1016/j.ecolmodel.200

Möllmann, C., Diekmann, R., Müller-Karulis, B., Kornilovs, G., Plikshs, M., & Axe, P. (2009). Reorganization of a large marine ecosystem due to atmospheric and anthropogenic pressure: A

discontinuous regime shift in the Central Baltic Sea. *Global Change Biology, 15*(6), 1377–1393. https://doi.org/10.1111/j.1365-2486.2008.01814.x

Moorcroft, P. R., Lewis, M. A., & Crabtree, R. L. (2006). Mechanistic home range models capture spatial patterns and dynamics of coyote territories in Yellowstone. *Proceedings of the Royal Society B, 273*(1594), 1651–1659. https://doi.org/10.1098/rspb.2005.3439

Morales-González, A., Fernández-Gil, A., Quevedo, M., Kramer-Schadt, S., Paniw, M., & Revilla, E. (2026). Resident mortality determines grey wolf range dynamics. *Journal of Applied Ecology, 63*, e70465. https://doi.org/10.1111/1365-2664.70465

Muñoz-Sabater, J., Dutra, E., Agustí-Panareda, A., Albergel, C., Arduini, G., Balsamo, G., … Thépaut, J.-N. (2021). ERA5-Land: A state-of-the-art global reanalysis dataset for land applications. *Earth System Science Data, 13*(9), 4349–4383. https://doi.org/10.5194/essd-13-4349-2021

Nordli, K., Wabakken, P., Eriksen, A., Sand, H., Wikenros, C., Maartmann, E., & Zimmermann, B. (2023). Spatial and temporal cohesion of parents and offspring in a social large carnivore. *Animal Behaviour, 197*, 155–167. https://doi.org/10.1016/j.anbehav.2022.12.006

Ordiz, A., Milleret, C., Kindberg, J., Månsson, J., Wabakken, P., Swenson, J. E., & Sand, H. (2015). Wolves, people, and brown bears influence the expansion of the recolonizing wolf population in Scandinavia. *Ecosphere, 6*(12), 284. https://doi.org/10.1890/ES15-00243.1

Perry, A. L., Low, P. J., Ellis, J. R., & Reynolds, J. D. (2005). Climate change and distribution shifts in marine fishes. *Science, 308*(5730), 1912–1915. https://doi.org/10.1126/science.1111322

Pimm, S. L. (1984). The complexity and stability of ecosystems. *Nature, 307*(5949), 321–326. https://doi.org/10.1038/307321a0

Recio, M. R., Singer, A., Wabakken, P., & Sand, H. (2020). Agent-based models predict patterns and identify constraints of large carnivore recolonizations, a case study of wolves in Scandinavia. *Biological Conservation, 251*, 108752. https://doi.org/10.1016/j.biocon.2020.108752

Recio, M. R., Zimmermann, B., Wikenros, C., Zetterberg, A., Wabakken, P., & Sand, H. (2018). Integrated spatially-explicit models predict pervasive risks to recolonizing wolves in Scandinavia from human-driven mortality. *Biological Conservation, 226*, 111–119. https://doi.org/10.1016/j.biocon.2018.07.025

Reinhart, V., Hoffmann, P., Rechid, D., Böhner, J., & Bechtel, B. (2022). High-resolution land use and land cover dataset for regional climate modelling: A plant functional type map for Europe 2015. *Earth System Science Data, 14*(4), 1735–1794. https://doi.org/10.5194/essd-14-1735-2022

Roberts, D. R., Bahn, V., Ciuti, S., Boyce, M. S., Elith, J., Guillera-Arroita, G., Hauenstein, S., Lahoz-Monfort, J. J., Schröder, B., Thuiller, W., Warton, D. I., Wintle, B. A., Hartig, F., & Dormann, C. F. (2017). Cross-validation strategies for data with temporal, spatial, hierarchical, or phylogenetic structure. *Ecography, 40*(8), 913–929. https://doi.org/10.1111/ecog.02881

Rodionov, S. N. (2004). A sequential algorithm for testing climate regime shifts. *Geophysical Research Letters, 31*(9), L09204. https://doi.org/10.1029/2004GL019448

Rufino, M. M., Bez, N., & Brind'Amour, A. (2018). Integrating spatial indicators in the surveillance of exploited marine ecosystems. *PLoS ONE, 13*(11), e0207538. https://doi.org/10.1371/journal.pone.0207538

Sand, H., Eklund, A., Zimmermann, B., Wikenros, C., & Wabakken, P. (2016). Prey selection of Scandinavian wolves: Single large or several small? *PLoS ONE, 11*(12), e0168062. https://doi.org/10.1371/journal.pone.0168062

Sand, H., Vucetich, J. A., Zimmermann, B., Wabakken, P., Wikenros, C., Pedersen, H. C., Peterson, R. O., & Liberg, O. (2012). Assessing the influence of prey–predator ratio, prey age structure and packs size on wolf kill rate. *Oikos, 121*(9), 1454–1463. https://doi.org/10.1111/j.1600-0706.2012.20082.x

Sand, H., Wikenros, C., Wabakken, P., & Liberg, O. (2006a). Cross-continental differences in patterns of predation: Will naive moose in Scandinavia ever learn? *Proceedings of the Royal Society B, 273*(1592), 1421–1427. https://doi.org/10.1098/rspb.2005.3447

Sanz-Pérez, A., Ordiz, A., Sand, H., Swenson, J. E., Wabakken, P., Wikenros, C., Zimmermann, B., Åkesson, M., & Milleret, C. (2018). No place like home? A test of the natal habitat-biased dispersal hypothesis in Scandinavian wolves. *Royal Society Open Science, 5*(12), 181379. https://doi.org/10.1098/rsos.181379

Scheffer, M., & Carpenter, S. R. (2003). Catastrophic regime shifts in ecosystems: Linking theory to observation. *Trends in Ecology & Evolution, 18*(12), 648–656. https://doi.org/10.1016/j.tree.2003.09.002

Sells, S. N., & Mitchell, M. S. (2020). The economics of territory selection. *Ecological Modelling, 438*, 109329. https://doi.org/10.1016/j.ecolmodel.2020.109329

Singh, N. J., & Ericsson, G. (2014). Changing motivations during migration: Linking movement speed to reproductive status in a migratory large mammal. *Biology Letters, 10*(6), 20140379. https://doi.org/10.1098/rsbl.2014.0379

Smithson, M., & Verkuilen, J. (2006). A better lemon squeezer? Maximum-likelihood regression with beta-distributed dependent variables. *Psychological Methods, 11*(1), 54–71. https://doi.org/10.1037/1082-989X.11.1.54

Tallian, A., Ordiz, A., Metz, M. C., Milleret, C., Wikenros, C., Smith, D. W., Stahler, D. R., Kindberg, J., MacNulty, D. R., Wabakken, P., Swenson, J. E., & Sand, H. (2017). Competition between apex predators? Brown bears decrease wolf kill rate on two continents. *Proceedings of the Royal Society B, 284*(1848), 20162368. https://doi.org/10.1098/rspb.2016.2368

Tallian, A., Ordiz, A., Metz, M. C., Zimmermann, B., Wikenros, C., Smith, D. W., Stahler, D. R., Wabakken, P., Swenson, J. E., Sand, H., & Kindberg, J. (2022). Of wolves and bears: Seasonal drivers of interference and exploitation competition between apex predators. *Ecological Monographs, 92*(2), e1498. https://doi.org/10.1002/ecm.1498

Taylor, L. R. (1961). Aggregation, variance and the mean. *Nature, 189*(4766), 732–735. https://doi.org/10.1038/189732a0

Trouwborst, A., Fleurke, F. M., & Linnell, J. D. C. (2017). Norway's wolf policy and the Bern Convention on European wildlife: Avoiding the "manifestly absurd". *Journal of International*

Wildlife Law & Policy, 20(2), 155–167. https://doi.org/10.1080/13880292.2017.1346013

Valavi, R., Elith, J., Lahoz-Monfort, J. J., & Guillera-Arroita, G. (2019). blockCV: An R package for generating spatially or environmentally separated folds for k-fold cross-validation of species distribution models. *Methods in Ecology and Evolution, 10*(2), 225–232. https://doi.org/10.1111/2041-210X.13107

Wabakken, P., Sand, H., Liberg, O., & Bjärvall, A. (2001). The recovery, distribution, and population dynamics of wolves on the Scandinavian peninsula, 1978–1998. *Canadian Journal of Zoology, 79*(4), 710–725. https://doi.org/10.1139/z01-029

Wabakken, P., Svensson, L., Maartmann, E., Nordli, K., Dupont, P., Milleret, C., Bischof, R., Åkesson, M., & Flagstad, Ø. (2026). *Bestandsovervåking av ulv vinteren 2025–2026. Inventering av varg vintern 2025–2026* (Bestandsstatus for store rovdyr i Skandinavia 1-2026). Rovdata and SLU Viltskadecenter.

Wikenros, C., Gicquel, M., Zimmermann, B., Flagstad, Ø., & Åkesson, M. (2021). Age at first reproduction in wolves: Different patterns of density dependence for females and males. *Proceedings of the Royal Society B, 288*(1948), 20210207. https://doi.org/10.1098/rspb.2021.0207

Wikenros, C., Liberg, O., Sand, H., & Åkesson, M. (2020). Impact of a recolonizing, cross-border carnivore population on ungulate harvest in Scandinavia. *Scientific Reports, 10*, 22124. https://doi.org/10.1038/s41598-020-78585-8

Woillez, M., Rivoirard, J., & Petitgas, P. (2009). Notes on survey-based spatial indicators for monitoring fish populations. *Aquatic Living Resources, 22*(2), 155–164. https://doi.org/10.1051/alr/2009017

Zimmermann, B., Nelson, L., Wabakken, P., Sand, H., & Liberg, O. (2014). Behavioral responses of wolves to roads: Scale-dependent ambivalence. *Behavioral Ecology, 25*(6), 1353–1364. https://doi.org/10.1093/beheco/aru134

Zimmermann, B., Sand, H., Wabakken, P., Liberg, O., & Andreassen, H. P. (2015). Predator-dependent functional response in wolves: From food limitation to surplus killing. *Journal of Animal Ecology, 84*(1), 102–112. https://doi.org/10.1111/1365-2656.12280